


# Recurrence quantification analysis of dynamic brain networks

Marinho A. Lopes<sup>1,2</sup>  | Jiaxiang Zhang<sup>2</sup> | Dominik Krzemiński<sup>2</sup> | Khalid Hamandi<sup>2</sup> | Qi Chen<sup>3</sup> | Lorenzo Livi<sup>4,5</sup> | Naoki Masuda<sup>1,6,7</sup>

<sup>1</sup>Department of Engineering Mathematics, University of Bristol, Bristol, UK

<sup>2</sup>Cardiff University Brain Research Imaging Centre, School of Psychology, Cardiff University, Cardiff, UK

<sup>3</sup>Center for Studies of Psychological Application and School of Psychology, South China Normal University, Guangzhou, China

<sup>4</sup>Departments of Computer Science and Mathematics, University of Manitoba, Winnipeg, MB, Canada

<sup>5</sup>Department of Computer Science, College of Engineering, Mathematics and Physical Sciences, University of Exeter, Exeter, UK

<sup>6</sup>Department of Mathematics, University at Buffalo, State University of New York, Buffalo, NY, USA

<sup>7</sup>Computational and Data-Enabled Science and Engineering Program, University at Buffalo, State University of New York, Buffalo, NY, USA

## Correspondence

Marinho A. Lopes, Department of Engineering Mathematics, University of Bristol, Bristol, UK.

Email: m.lopes@exeter.ac.uk

Naoki Masuda, Department of Mathematics, University at Buffalo, State University of New York, NY, USA.

Email: naokimas@buffalo.edu

## Funding information

National Natural Science Foundation of China, Grant/Award Number: 31871138; GW4 Accelerator Fund; Engineering and Physical Sciences Research Council, Grant/Award Number: EP/N509449/1; Chang Jiang Scholars Program (2016); Canada Research Chairs program; H2020 European Research Council, Grant/Award Number: 716321; AFOSR European Office, Grant/Award Number: FA9550-19-1-7024; Wales BRAIN Unit; Health and Care Research Wales: Clinical Research Time Award

## Abstract

Evidence suggests that brain network dynamics are a key determinant of brain function and dysfunction. Here we propose a new framework to assess the dynamics of brain networks based on recurrence analysis. Our framework uses recurrence plots and recurrence quantification analysis to characterize dynamic networks. For resting-state magnetoencephalographic dynamic functional networks (dFNs), we have found that functional networks recur more quickly in people with epilepsy than in healthy controls. This suggests that recurrence of dFNs may be used as a biomarker of epilepsy. For stereo electroencephalography data, we have found that dFNs involved in epileptic seizures emerge before seizure onset, and recurrence analysis allows us to detect seizures. We further observe distinct dFNs before and after seizures, which may inform neurostimulation strategies to prevent seizures. Our framework can also be used for understanding dFNs in healthy brain function and in other neurological disorders besides epilepsy.

## KEYWORDS

epilepsy, functional network, MEG, stereo EEG

## 1 | INTRODUCTION

The brain is a complex dynamic system. To map, model and study brain structure and function, it is useful to define

brain networks (Bassett & Sporns, 2017; Fornito, Zalesky, & Bullmore, 2016). The study of brain networks has transformed our understanding of the brain, and it has the potential to revolutionize the clinical management of neurological disorders

**Abbreviations:** dFN, dynamic functional networks; JME, juvenile myoclonic epilepsy; RP, recurrence plot; RQA, recurrence quantification analysis; sEEG, stereo EEG.

This is an open access article under the terms of the Creative Commons Attribution License, which permits use, distribution and reproduction in any medium, provided the original work is properly cited.

© 2020 The Authors. *European Journal of Neuroscience* published by Federation of European Neuroscience Societies and John Wiley & Sons Ltd.

(Stam, 2014). Two main types of brain networks have been considered: structural and functional networks (Bullmore & Sporns, 2009; Sporns, 2013). Structural networks describe the anatomical connectivity of the brain and are relatively stable on short time scales (i.e. s to min). In contrast, functional networks are inferred from statistical dependencies between neural signals recorded from different brain regions. Statistical dependencies are then assumed to represent functional couplings between brain regions. The statistical dependencies between signals are not stationary, making functional networks time-dependent on short time scales (tens or hundreds of milliseconds; Sporns, 2013). A growing body of evidence shows that dynamic functional networks (dFNs) capture crucial aspects underlying normal function and dysfunction of the brain (Calhoun, Miller, Pearlson, & Adali, 2014; Cohen, 2018; Hutchison et al., 2013). In particular, epilepsy, which will be the focus of this study, has been considered to be a dynamical disease of the brain (da Silva et al., 2003), and dFNs have been useful for characterizing the epileptic brain (Lehnertz et al., 2014).

A number of different approaches have been employed to study dFNs (Braun et al., 2018; Hutchison et al., 2013). A common approach has been to calculate some measures from the functional networks and track their changes over time (Fuertinger, Simonyan, Sperling, Sharan, & Hamzei-Sichani, 2016; Kramer et al., 2010; Lehnertz et al., 2014; Schindler, Bialonski, Horstmann, Elger, & Lehnertz, 2008). For example, a time-dependent analysis of the average shortest path length and the clustering coefficient revealed that functional networks evolve from a more random topology before seizures towards a more regular topology during seizures and back to a more random topology after seizure offset (Schindler et al., 2008). This approach is limited by an a priori choice of measures that may or may not fully characterize the dynamics of the functional networks. Another common approach is to use a Bayesian framework to characterize dFNs. In particular, hidden Markov models have been employed to analyse dFNs (Eavani, Satterthwaite, Gur, Gur, & Davatzikos, 2013; Sourty et al., 2016; Vidaurre et al., 2018). For example, product hidden Markov models have been used to identify brain networks involved in dementia with Lewy bodies (Sourty et al., 2016). This approach makes the assumption that the dynamics of the state is Markovian, i.e. the transition between different states is a memoryless stochastic process. However, long-term correlations in temporal patterns of brain activity suggest that this assumption may not always hold (Chialvo, 2010; Ezaki, Dos Reis, Watanabe, Sakaki, & Masuda, 2020; Kitzbichler, Smith, Christensen, & Bullmore, 2009). Thus, these approaches make assumptions that may hinder a comprehensive assessment of the dynamics of functional networks.

Recurrence is a key concept in dynamical systems (Eckmann, Kamphorst, & Ruelle, 1995; Marwan, Romano, Thiel, & Kurths, 2007). It was first introduced by Henri Poincaré in 1,890 and it can be used to characterize a system's

dynamical behaviour. In the late 1980s, Eckmann et al. introduced the *recurrence plot* (RP), a tool to visualize the recurrences of a dynamical system (Eckmann, Kamphorst, & Ruelle, 1987). Subsequently, *recurrence quantification analysis* (RQA) emerged as a means to quantify RPs (Marwan et al., 2007). RQA has been applied to a range of dynamical systems and empirical data (Marwan et al., 2007; Webber & Marwan, 2015). In particular, RQA has been used for examining brain activity (see e.g. Ngamga et al., 2016; Ouyang, Li, Dang, & Richards, 2008; Shabani, Mikaili, & Noori, 2016; Yan, Feng, Dai, & Wang, 2016; Yang, Luan, Liu, & Wang, 2019). RQA has been used for the identification of pre-seizure states from intracranial EEG data recorded from people with epilepsy (Ngamga et al., 2016), and for distinguishing EEG signals between healthy individuals and people with epilepsy (Yan et al., 2016). More recently, RQA indicated that the epileptogenic zone produces more deterministic dynamics than other brain regions (Yang et al., 2019). However, these approaches, including the application of RP and RQA to other neural data, neglect the spatial dependencies between the neural signals, i.e. they do not assess the recurrence of the underlying functional networks.

In this study, we propose methods of RP and RQA for dFNs. While the methods may be used to explore dFNs from various neurological disorders, here we focus on epilepsy. Functional networks may be crucial for understanding epilepsy (Richardson, 2012). As functional brain networks are dynamic and epilepsy is a dynamical disease, RQA of dynamical functional networks may be particularly useful to characterize the epileptic brain. We use two data sets. The first one comprises MEG resting-state signals from people with a generalized epilepsy syndrome, Juvenile Myoclonic Epilepsy (JME) and healthy controls. Our aim is to test whether dFNs differ between the two groups, and whether this can be used as a biomarker of JME. The second data set comprises invasive stereo EEG (sEEG) recordings from people with drug-resistant focal epilepsy. Using this data set, we aim to assess functional network dynamics before, during and after seizures, particularly examining whether functional networks before seizures recur during and after seizures and across different seizures. We also assess whether RQA of dFNs may be used to automatically detect seizures. The application of our methods to these two data sets allows us to show the methods' flexibility and versatility, which in turn enables us to test the range of different hypotheses just described.

## 2 | MATERIALS AND METHODS

Our framework to study dynamic brain networks comprises five key steps (Figure 1): (a) use a sliding window approach to segment data from MEG or EEG recordings (Figure 1a); (b) infer a functional network from each segment of data

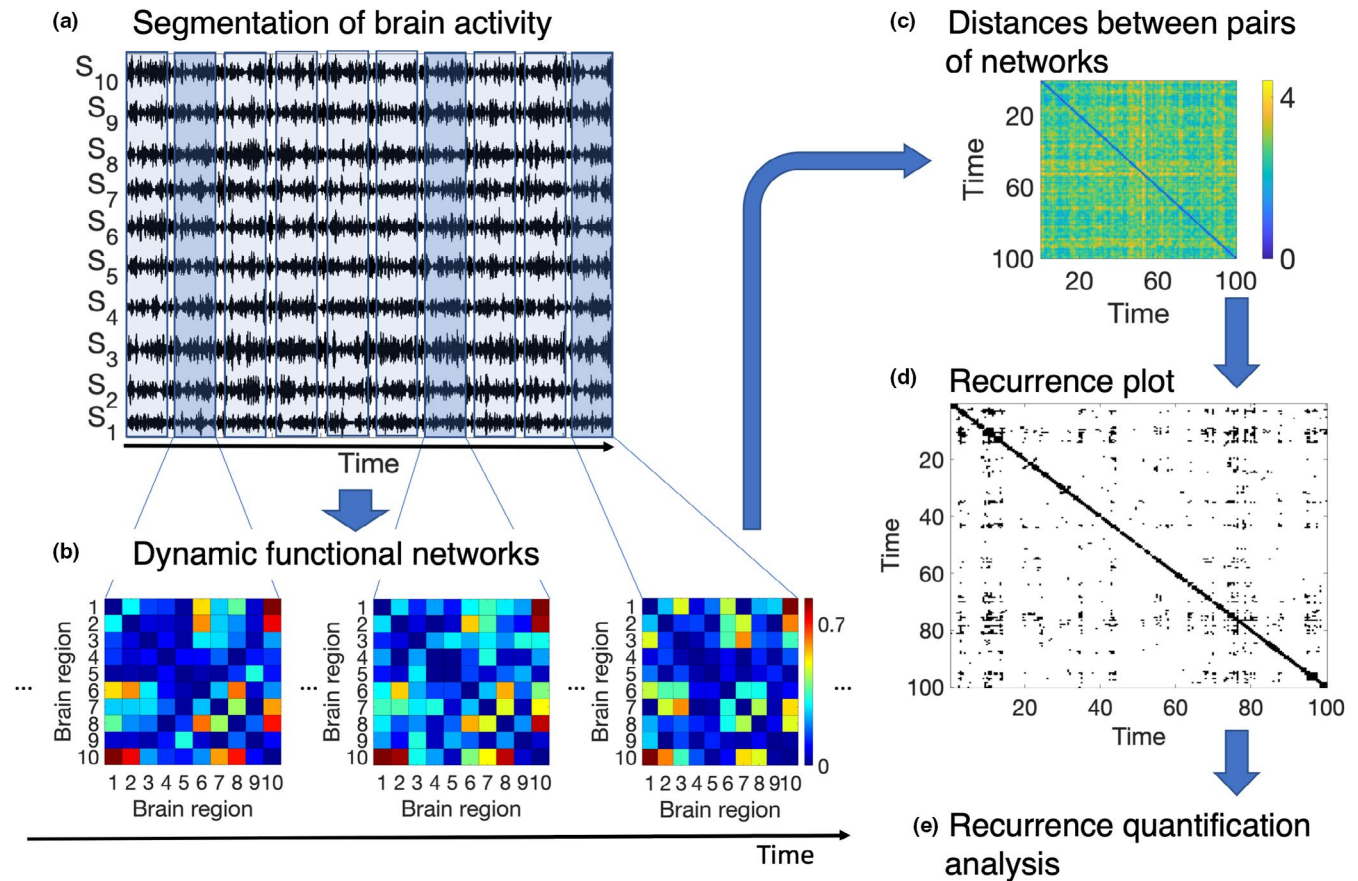


**FIGURE 1** Scheme of the data analysis procedure to apply recurrence quantification analysis to dynamic functional brain networks. (a) We segment brain activity into windows. (b) From each window, we infer a functional brain network. (c) We employ a distance measure for assessing the similarity between functional networks at each pair of time windows, resulting in a distance matrix. (d) We obtain a recurrence plot by assessing the distances between functional networks. Black dots correspond to entries in the distance matrix shown in (c) whose value is smaller than a threshold. (e) We then use recurrence quantification analysis to interrogate the recurrence plot and consequently characterize the dynamics of the functional networks. Note that, in our analysis, the windows represented in (a) overlapped with adjacent windows. In this figure, we avoided representing overlapping windows for visual clarity

(Figure 1b); (c) compute the distance between pairs of functional networks (Figure 1c); (d) apply a threshold to the pairwise distances and obtain a recurrence plot (RP; Figure 1d); and (e) perform recurrence quantification analysis (RQA) to extract information from the RP (Figure 1e).

## 2.1 | Data acquisition and pre-processing

We study two data sets from patients with epilepsy: one comprising MEG recordings and the other containing stereo EEG (sEEG) recordings.

### 2.1.1 | MEG recordings

We consider resting-state MEG data recorded from 26 people with JME and 26 healthy controls. The people with epilepsy were recruited from a specialist clinic for epilepsy at

University Hospital of Wales in Cardiff, and the healthy controls were volunteers who had no history of significant neurological or psychiatric disorders. The two groups were age and gender matched (age range [19, 45], median 27 years, and 8 males in the epilepsy group; age range [18, 48], median 27, and 7 males in the control group). People with epilepsy had a number of different seizure types and were taking anti-epileptic drugs (see Krzemiński et al., 2020 for more details about this data set). MEG data were acquired using a 275-channel CTF radial gradiometer system (CTF System, Canada) at a sampling rate of 600 Hz. Recording sessions lasted for approximately 5 min per individual. The participants were instructed to sit steadily in the MEG chair with their eyes focused on a red dot on a grey background. The participants also underwent a whole-brain T1-weighted MRI acquired using a General Electric HDx 3T MRI scanner and an 8-channel receiver head coil (GE Healthcare) with an axial 3D fast spoiled gradient recalled sequence (echo time 3 ms; repetition time 8 ms; inversion time 450 ms; flip

angle 20°; acquisition matrix 256 × 192 × 172; voxel size 1 × 1 × 1 mm). This study was approved by the South East Wales NHS ethics committee, Cardiff and Vale Research and Development committees, and Cardiff University School of Psychology Research Ethics Committee. Written informed consent was obtained from all participants.

The data were first divided into 2 s segments and then each segment was visually inspected to remove motion, muscle and eye-blink artefacts, and also inter-ictal spike wave discharges from the MEG recordings. Artefact-free segments were identified and re-concatenated for each subject. The resulting epochs had variable lengths ranging from 204 to 300 s. The pre-processed data were then filtered in the classical frequency bands (theta (4–7 Hz), alpha (8–13 Hz), beta (15–25 Hz) and gamma (30–60 Hz) bands), and down-sampled to 250 Hz.

### 2.1.2 | sEEG recordings

We also used a data set comprising 10 people with drug-resistant focal epilepsy who underwent invasive monitoring with stereo EEG at the 999 Brain Hospital, China. Stereo EEG is an advanced procedure in the epilepsy surgery evaluation, to help delineate the irritative and seizure onset zones, and hence decide the suitability and plan epilepsy surgery (Duncan, Winston, Koepp, & Ourselin, 2016). The age range of the group was [16,31], median 23, and nine individuals were males. Electrode implantation locations were personalized according to imaging and non-invasive EEG data; the number of electrodes per implantation ranged from five to 16, and each electrode had two to 16 contacts (i.e. channels). Four individuals received bilateral implantations, two individuals had electrodes implanted in their right hemispheres, and the other four individuals received implantations in their left hemispheres. Stereo EEG data were acquired using Nihon Kohden recording system at a sampling rate of 1 or 2 kHz. For all individuals, high-resolution T1-weighted MRI were acquired before electrode implantation, and computed tomography (CT) was acquired after electrode implantation. Co-registration of the CT to the MR images allowed us to determine whether contacts were placed in grey matter. All individuals had at least two seizures recorded. Seizure onset was defined by epileptologists at the 999 Brain Hospital and corroborated by one of the authors (KH) who also marked seizure offset. This study was approved by 999 Brain Hospital ethics committee and South China Normal University ethics committee. Written informed consent was obtained from all participants.

We restricted our analysis to artefact-free sEEG channels placed on grey matter as established from co-registration of the CT scans to the MRIs. (Artefact-free channels were

identified by KH) The number of channels  $N_{ch}$  considered per individual ranged from 19 to 83 (median 63.5). We selected peri-ictal epochs of data containing 300 s before seizure onset (pre-ictal), seizure (ictal), and 300 s after seizure offset (post-ictal). We then neglected peri-ictal epochs whose pre-ictal 300 s overlapped with the post-ictal 300 s of the previous peri-ictal epoch. Thus, we end up with 2–4 peri-ictal epochs per individual (three individuals had 2 epochs each; five individuals had 3 epochs each; and two individuals had 4 epochs each, making a total of 29 peri-ictal epochs). The data were re-referenced to the average of all artefact-free channels, filtered in a broad frequency band (0.5–120 Hz), which encapsulates the traditional clinical frequency bands (delta, theta, alpha, beta and gamma Buzsáki, 2006), notch filtered to remove power line interference (48–52 Hz) and down-sampled to 250 Hz.

## 2.2 | Inferring functional networks

The first step of the method is to construct dFNs. In this section we describe how we segmented the pre-processed MEG and sEEG data and inferred a functional network from each segment.

### 2.2.1 | Dynamic MEG functional networks in the source space

To compute functional networks from the MEG data, we first transformed the MEG recordings from the sensor space to the source space. This procedure consisted of co-registering the MEG sensors with the structural MRI using the locations of the fiducial coils in the CTF software (MRIVIEWER and MRICONVERTER). Then, we inferred a volume conduction model from the MRI scan using a semi-realistic model (Nolte, 2003). Finally, we reconstructed the source signals from the sensor signals using a linear constrained minimum variance (LCMV) beamformer on a 6-mm template with a local-spheres forward model in Fieldtrip (Oostenveld, Fries, Maris, & Schoffelen, 2011; <http://www.ru.nl/neuroimaging/fieldtrip>). Sources were mapped into the 90 brain regions of the Automated Anatomical Label (AAL) atlas (Hipp, Hawellek, Corbetta, Siegel, & Engel, 2012). More details about these methods have been provided in our previous study (Krzemiński et al., 2020).

To compute dFNs, we divided the 90-dimensional source reconstructed MEG signals into segments, each of which was composed of 500 samples (i.e. 2 s). Each segment was subsequently used for constructing one functional network. The choice of segment length balances the need for a sufficient number of samples to infer a reliable functional network and the need for a sufficiently large number of functional networks,



$M$ , for analysing their recurrence over time. The segment size of 500 is within a typical range in both MEG and EEG studies of functional connectivity (see e.g. Colclough et al., 2016; Khambhati et al., 2015; Stahn & Lehnertz, 2017). We set the overlap between consecutive segments to be 80% such that consecutive segments shared 400 samples, i.e. 1,600 ms. Therefore, the time step between consecutive dFNs was 100 samples, i.e. 400 ms. This choice represents a compromise between the need for sufficiently many networks for subsequent analysis, which is satisfied with a large overlap, and the need for avoiding trivial recurrences between consecutive functional networks. See Supporting Information S1 for computational results underlying the choice of the 80% overlap. The MEG data had different lengths for different participants. Therefore, we only considered the first  $M=506$  segments, which was the minimum number of segments among all participants, to exclude the potential impact of different recording lengths on our results.

For each segment, we built two functional networks using two established methods (Colclough et al., 2016): phase lag index (PLI; Stam, Nolte, & Daffertshofer, 2007) and amplitude envelope correlation (AEC) with orthogonalized signals (Hipp et al., 2012; see Supporting Information S2 for more details). We selected the PLI and AEC because they measure different types of intrinsic coupling, one related to phase coupling, and the other to amplitude correlations. They are expected to complement each other in describing brain network interactions (Engel, Gerloff, Hilgetag, & Nolte, 2013; Guggisberg et al., 2015). Note that as we considered four frequency bands for each definition of functional connectivity (i.e. PLI and AEC), we obtained eight sequences of matrices  $\mathbf{A}(t)=(a_{ij}(t))$ , where  $i, j=1, \dots, 90$ , and  $t=1, \dots, 506$ . Each matrix  $\mathbf{A}(t)$  represented a functional network for segment  $t$ , and matrix entry  $a_{ij}(t)$  represented the strength of the functional connectivity between regions  $i$  and  $j$ . Each matrix  $\mathbf{A}(t)$  was symmetric, i.e. the functional networks were undirected.

### 2.2.2 | Dynamic sEEG functional networks in the sensor space

Following the same procedure as the one employed for the MEG data, we divided each of the 29 sEEG peri-ictal epochs into segments of 500 samples (i.e. 2 s) using an overlap of 400 samples between consecutive segments. Because different peri-ictal epochs contained seizures of different lengths (from 9 to 181 s, median 75 s), different peri-ictal epochs resulted in different numbers of segments  $M$  (from 1542 to 1822, median 1632).

Because the sEEG data were recorded intracranially close to the brain sources, we computed functional networks in the sensor space, i.e. using the channels as network nodes and functional connections as the statistical dependencies between

the signals recorded at the channels. For each segment, we inferred a functional network using the absolute value of the Pearson's correlation coefficient between pairs of channels (Lopes et al., 2017; Rummel et al., 2015; Rummel, Müller, Baier, Amor, & Schindler, 2010). These methods differ from those applied to the MEG data because the two data modalities are different with regard to volume conduction. Volume conduction is a confounding factor in non-invasive data and is responsible for spurious zero-lag correlations (Bastos & Schoffelen, 2016). Thus, while we had to use methods capable of accounting for volume conduction in the MEG data set, such a concern does not apply to invasive sEEG data, for which the Pearson's correlation based on broadband signals is a reliable method (Rummel et al., 2010). The Pearson's correlation is considered to be the simplest measure to capture possible linear relationships between two signals (Bastos & Schoffelen, 2016). Thus, we obtained 29 time-varying matrices  $\mathbf{A}(t)=(a_{ij}(t))$  of size  $(N_{\text{ch}} \times N_{\text{ch}})$ , where  $t=1, \dots, M$ , representing functional networks through pre-ictal, ictal and post-ictal periods. Note that the number of channels,  $N_{\text{ch}}$ , was fixed for each individual, but  $M$  varied from one peri-ictal epoch to another even for a single individual due to seizure of different lengths.

### 2.3 | Recurrence plots and distance measures

The second step of the method is to obtain an RP from a dFN.

For a dynamical system characterized by a vector time series  $\vec{x}(t)$ , where  $t=1, \dots, M$ , an  $M \times M$  recurrence matrix is defined as

$$R_{t_1, t_2} = \begin{cases} 1 & \text{if } d(\vec{x}(t_1), \vec{x}(t_2)) \leq \epsilon \\ 0 & \text{if } d(\vec{x}(t_1), \vec{x}(t_2)) > \epsilon \end{cases}, \quad (1)$$

where  $d(\vec{x}(t_1), \vec{x}(t_2))$  is a distance measure between  $\vec{x}(t_1)$  and  $\vec{x}(t_2)$ , and  $\epsilon$  is a small distance which defines an upper limit of discrepancy between recurrent states (Marwan, Donges, Zou, Donner, & Kurths, 2009; Marwan et al., 2007). The recurrence matrix is a symmetric matrix, and its main diagonal entries are equal to 1.

To compute RPs of dFNs, we replaced the vectors  $\vec{x}(t_a)$  by matrices  $\mathbf{A}(t_a)$  and used distance measures for pairs of weighted networks (i.e. matrices). The recurrence matrix for a dFN is given by

$$R_{t_1, t_2} = \begin{cases} 1 & \text{if } d(\mathbf{A}(t_1), \mathbf{A}(t_2)) \leq \epsilon \\ 0 & \text{if } d(\mathbf{A}(t_1), \mathbf{A}(t_2)) > \epsilon \end{cases}, \quad (2)$$

where  $d(\mathbf{A}(t_1), \mathbf{A}(t_2))$  is the distance between functional networks  $\mathbf{A}(t_1)$  and  $\mathbf{A}(t_2)$  measured according to a distance measure for networks. There is a variety of distance measures for networks (Livi & Rizzi, 2013), but a good choice for functional networks is unknown. We therefore used six distance measures to obtain six different RPs per dFN. The use of multiple distance measures aimed at not missing potentially useful information provided by different, yet arbitrary choices of distance measures. We considered the Frobenius norm, the log-Euclidean distance, the spectral norm, the Euclidean norm between Fiedler vectors, the maximum norm between the Fiedler vectors and the cosine dissimilarity between the Fiedler vectors. We then assessed whether these distance measures were actually complementing each other or being redundant (we will return to this issue in Section 2.5 below). We reduced the number of distance measures to three of interest: the Frobenius norm, the spectral norm and the Euclidean norm between Fiedler vectors. These measures were applied to pairs of networks and are defined as follows.

The Frobenius norm of the difference between a pair of networks is given by (Kurmukov, Dodonova, & Zhukov, 2016).

$$d_F(\mathbf{A}(t_1), \mathbf{A}(t_2)) = \|\mathbf{A}(t_1) - \mathbf{A}(t_2)\|_F = \sqrt{\sum_{i=1}^N \sum_{j=1}^N (a_{ij}(t_1) - a_{ij}(t_2))^2}. \quad (3)$$

This distance measure is the Euclidean distance between the two networks when they are represented as  $M^2$ -dimensional vectors.

The spectral norm of the difference between a pair of networks is given by

$$d_S(\mathbf{A}(t_1), \mathbf{A}(t_2)) = \sqrt{\lambda_{\max}\{[\mathbf{A}^*(t_1) - \mathbf{A}^*(t_2)][\mathbf{A}(t_1) - \mathbf{A}(t_2)]\}}, \quad (4)$$

where  $\lambda_{\max}\{\bullet\}$  is the largest eigenvalue of the matrix, and  $\mathbf{A}^*(t)$  is the conjugate transpose of  $\mathbf{A}(t)$  (Miller, Stephens, & Bliss, 2012). In fact, our matrices  $\mathbf{A}(t)$  are real, and therefore  $\mathbf{A}^*(t)$  is just the transpose of  $\mathbf{A}(t)$ .

The third measure is the Euclidean norm between Fiedler vectors, which, as the name suggests, is based on spectral properties of the Laplacian networks, specifically their Fiedler vectors. The Fiedler vector of a network is the eigenvector corresponding to the smallest positive eigenvalue of the Laplacian matrix of the network, which is often referred to as the algebraic connectivity of the network. The use of the Laplacian matrix is motivated by evidence showing that the Laplacian matrix is better for computing spectral distances than the adjacency matrix (Wilson & Zhu, 2008). The Fiedler vector characterizes the partitioning of the network into communities (Newman, 2006). Here, we considered the so-called symmetric normalized Laplacian

matrix given by  $\mathbf{L}'(t_a) = \mathbf{D}^{-1/2}(t_a) \mathbf{L}(t_a) \mathbf{D}^{-1/2}(t_a)$ , where  $\mathbf{L}(t_a) = \mathbf{D}(t_a) - \mathbf{A}(t_a)$  is the combinatorial Laplacian, and  $\mathbf{D}(t_a)$  is a diagonal matrix whose main diagonal entries are given by  $d_{ii}(t_a) = \sum_{j=1}^N a_{ij}(t_a)$ . We denote the normalized Fiedler vector of  $\mathbf{L}'(t)$  by  $\vec{v}(t) = (v_1(t), v_2(t), \dots, v_N(t))^T$  where  $T$  represents the transposition. To compute the distance between the normalized Fiedler vectors  $\vec{v}(t_1)$  and  $\vec{v}(t_2)$ , we used the Euclidean norm between Fiedler vectors given by

$$d_{EF}(\mathbf{A}(t_1), \mathbf{A}(t_2)) = \sqrt{\sum_{k=1}^N (v_k(t_1) - v_k(t_2))^2}. \quad (5)$$

We used the appropriate orientation of the Fiedler vectors to calculate these distance measures (see the Supporting Information S3 for more details). For details about the other three distance measures, see Supporting Information S4.

To obtain an RP for each distance measure, one needs to define a threshold  $\epsilon$ . The value of  $\epsilon$  may have a crucial impact on the structure of the RP (Marwan et al., 2007). We used  $\epsilon$  such that the density of points in the RPs was fixed. In other words, all RPs had the same ratio of the number of recurrences to  $M(M-1)$ , the total number of possible recurrences. (Recurrence points along the main diagonal are ignored because they are trivial) The advantage of this choice is the opportunity to compare the structure of different RPs, because such comparisons are only meaningful if the RPs have the same density of points (Marwan et al., 2007). We ran our analysis for three different thresholds such that the density of points was 0.01, 0.05 and 0.10 respectively.

## 2.4 | Recurrence quantification analysis

The third step of the method is to quantify the structure of the RPs, which allows us to characterize the dynamics of the functional networks and compare different dFNs. For this purpose, we employed 12 RQA measures (Marwan et al., 2007), i.e. 11 out of the 13 measures implemented in version 5.22 of the CRP toolbox for MATLAB provided by TOCSY: <http://tocsy.agnld.uni-potsdam.de>, and the  $\tau$ -recurrence rate (denoted by  $RR_\tau$ ). For a full description of the measures in the CRP toolbox, see Supporting Information S6. We excluded the recurrence rate, i.e. the density of recurrence points in an RP, because we fixed this quantity to set the threshold,  $\epsilon$ , to build the RPs. We also excluded the clustering (*clust*) because it was generally small or undefined in our RPs due to the relatively low density of points in the RPs.

Among the 11 RQA measures in the CRP toolbox, four are based on the diagonal lines of the RPs, which result from recurring sequences of adjacent functional networks: the

determinism ( $DET$ ), the mean diagonal line length ( $\langle L \rangle$ ), the maximal diagonal line length ( $L_{\max}$ ) and the entropy of the diagonal line lengths ( $ENTR$ ). In the analysis of the sEEG data set, we will highlight the  $DET$ ,  $\langle L \rangle$  and  $L_{\max}$ . A larger value of these measures implies that the dFNs are more ‘deterministic’. Here, higher ‘determinism’ means that the dFNs have longer consecutive sequences of functional networks that repeat at different times (Marwan et al., 2007).

Three other RQA measures quantify the vertical lines composed of recurrent points in the RPs, which represent time intervals in which the networks do not considerably change: the laminarity ( $LAM$ ), the trapping time ( $TT$ ) and the maximal vertical line length ( $V_{\max}$ ). Among these measures, we will particularly focus on the  $TT$  in Section 3.1. It is equal to the average length of vertical lines in the RP. A large  $TT$  value implies that the dFNs are more likely to be trapped into specific functional networks at any given time.

Another three RQA measures assess the recurrence times, i.e. the vertical distance between recurrence points in the RPs: the recurrence time of first type ( $T1$ ), the recurrence time of second type ( $T2$ ) and the recurrence time entropy ( $RT_E$ ). We highlight  $T1$  and  $T2$  in Section 3.1. They quantify the average time that functional networks take to approximately recur to a previous network. The difference between  $T1$  and  $T2$  is that  $T2$  neglects recurrence times equal to 1 which may correspond to spurious recurrences (see Supporting Information S6 for more details).

The final RQA measure assesses the RP by regarding it as a network: the transitivity ( $Trans$ ). These RQA measures quantify different aspects of the temporal dynamics enclosed in the RPs. We used the CRP toolbox provided by TOCSY to compute these RQA measures. These 11 measures were used to assess the MEG data set and to compare pre- and post-ictal periods in the sEEG data set.

The  $RR_\tau$  was used to assess peri-ictal epochs in the sEEG data set. It is given by

$$RR_\tau = \frac{1}{M-\tau} \sum_{t=1}^{M-\tau} R_{t,t+\tau}. \quad (6)$$

This measure counts the number of recurrence points on diagonal lines with a distance  $\tau$  from the main diagonal. The  $RR_\tau$  can be considered as a generalized auto-correlation function (Marwan et al., 2007). To facilitate the interpretation of this measure, for each RP, we also computed 100 randomly shuffled RPs. We generated randomly shuffled RPs by taking the  $(M-1)(M-2)/2$  matrix entries from the upper triangular part of the original RP matrix, uniformly randomly shuffling these entries and then constructing a symmetric matrix using the shuffled upper triangular part and the main diagonal entries set to zero. Then, we computed the  $RR_\tau$  value for each randomly shuffled RP, which we denote by  $RR_\tau^{\text{null}}$ . By calculating the mean and standard deviation of  $RR_\tau^{\text{null}}$  at each  $\tau$ ,

based on the 100 samples, we obtained a reference to assess whether  $RR_\tau$  deviated from chance at each  $\tau$ .

To assess the variation in RQA measures between pre- and post-ictal periods in the same peri-ictal epoch in the sEEG data, we computed  $\Delta X = (X_{\text{post}} - X_{\text{pre}}) / (X_{\text{pre}} + X_{\text{post}})$ , where  $X_{\text{pre}}$  is an RQA measure calculated based on the pre-ictal RP, and  $X_{\text{post}}$  is the same RQA measure calculated based on the post-ictal RP. Note that  $\Delta X$  varies between  $-1$  and  $1$ . Values close to  $-1$  imply  $X_{\text{pre}} \gg X_{\text{post}}$ , values close to  $1$  imply  $X_{\text{pre}} \ll X_{\text{post}}$  and values close to  $0$  imply  $X_{\text{pre}} \approx X_{\text{post}}$ .

## 2.5 | Reduction in the number of configurations

Thus far, our method comprised multiple methodological choices (i.e. different frequency bands, functional network measures, network distance measures and threshold values), which may yield redundant RPs and consequently redundant RQA results. To avoid such redundant information and inefficient computations, we reduced the number of methodological choices as follows.

In particular, for the MEG data set, we considered four frequency bands, two functional network measures, six network distance measures and three threshold values. Different combinations of these four factors yield different RPs. However, we observe that a majority of these RPs may be redundant. Therefore, we selected representative RPs as follows. For clarity, we define a configuration as one combination of frequency band, functional network and distance measure; we will separately consider the threshold. For example, the combination of the alpha frequency band, PLI and the Frobenius norm is a configuration. We assessed whether some of the  $4 \times 2 \times 6 = 48$  configurations yielded redundant RPs by comparing RQA results obtained using different configurations. We studied the relations among the 48 configurations for three randomly selected healthy controls from the MEG data set, using Pearson's correlation between RQA values across configurations (see Supporting Information S5 for details). This investigation yielded a few representative configurations whose RPs we used for the subsequent analysis. We carried out this assessment of configurations independently for each of the three threshold values because, as mentioned, RPs are threshold-dependent and comparisons between RPs with different thresholds are not meaningful.

## 2.6 | Statistical methods

We used the Mann–Whitney  $U$  test to assess whether the median of each RQA measure was different between the epilepsy and control groups in the MEG data set. We applied Bonferroni–Holm correction to correct p-values due to

multiple comparisons across different configurations. We considered that the four configurations provided a family of four hypotheses for which we accounted the familywise error rate by correcting the  $p$ -values in the family. We did not correct  $p$ -values across the RQA measures because we considered that these tests corresponded to different families of hypotheses.

To evaluate whether RQA measures significantly changed from pre-ictal to post-ictal epochs in the sEEG data set, we used the Wilcoxon signed-rank test.

## 2.7 | Classification methods

We further used RQA measures to classify individuals as to whether they had epilepsy in the MEG data set. We employed MATLAB's Classification Learner Toolbox which comprises a suite of 24 different classifiers, including logistic regression, trees,  $k$  nearest neighbour (kNN), among others. We tested the capability of different RQA measures and different configurations to classify the two groups of people. For each test we used all 24 classifiers in MATLAB's toolbox and chose the one with highest accuracy. We further tested whether combining all RQA measures from the four configurations yielded a higher accuracy. Because in this case we would be attempting a classification of 52 individuals using a relatively large number of features (44 features from 4 configurations  $\times$  11 RQA measures), we first reduced the number of features by using principal component analysis (PCA). Not to bias the principal components towards RQA measures with higher variances, we normalized the features. To avoid overfitting, we employed a 50-fold cross-validation procedure in all these classifications, which is a feature of the MATLAB's toolbox. The cross-validation consisted in partitioning the 52 individuals into 48 groups of one individual and two groups of two individuals, and then training the classifiers with 49 groups and testing them using the remaining group. We repeated this training-and-test procedure 50 times such that each group was used just once for testing.

## 3 | RESULTS

We applied our methods to two different data sets, a MEG and a sEEG data set. Our purpose was to test the usefulness of the methods in the assessment of dFNs in different contexts, enabling us to explore different strengths of the methods and allowing us to test a number of hypotheses in each data set.

### 3.1 | Dynamic MEG functional networks

We studied the dynamics of functional networks inferred from resting-state MEG data and tested whether dFNs from

people with epilepsy differ from healthy controls. We considered signals filtered in four frequency bands, two functional connectivity measures (i.e. AEC and PLI) and six distance measures between pairs of networks. We defined a configuration as a combination of a frequency band, connectivity measure and distance measure. We first studied the relations between the different configurations and observed that four configurations were sufficiently representative of all the configurations (see Supporting Information S5). All of these four configurations were in the theta band. Three of them used the AEC as connectivity measure, whereas the other one used the PLI. The three representative distance measures identified together with the AEC were the Frobenius norm ( $d_F$ , Equation 3), the spectral norm ( $d_S$ , Equation 4) and the Euclidean norm between the Fiedler vectors ( $d_{EF}$ , Equation 5). The representative distance measure identified together with the PLI was the spectral norm. We denote these four configurations by AEC +  $d_F$ , AEC +  $d_S$ , AEC +  $d_{EF}$  and PLI +  $d_S$ .

We used our recurrence analysis framework to compare the dynamics of resting-state MEG functional networks between people with epilepsy and healthy controls. First, we considered the AEC +  $d_F$  configuration. For each individual, we obtained a sequence of 506 functional networks using AEC as connectivity measure (Figure 1b). We then computed the distance between each pair of networks using  $d_F$  as distance measure, obtaining a distance matrix (Figure 1c). Next, we identified a threshold such that 5% of the points in the distance matrix apart from the main diagonal had a distance smaller than the threshold. By thresholding the distance matrix, we obtained an RP (Figure 1d). Figure 2a,b show RPs from a healthy individual and an individual with epilepsy respectively. We then used the 11 RQA measures to compare the RPs between the healthy and epilepsy groups. For example, Figure 2c compares the trapping time ( $TT$ ), an RQA measure, between the two groups using the AEC +  $d_F$  configuration. We then tested whether the median of each RQA measure was different between the two groups using the Mann–Whitney  $U$  test. We found that the recurrence time of first type ( $T1$ ) and the recurrence time of second type ( $T2$ ) were smaller in people with epilepsy than in controls in the AEC +  $d_F$  configuration (see Figure 2g,k).

We repeated the same analysis for the other three configurations. Overall, we observed smaller  $T1$  and  $T2$  in people with epilepsy than in controls in the AEC +  $d_F$  and AEC +  $d_S$  configurations;  $T1$  was higher in people with epilepsy than controls in the AEC +  $d_{EF}$  configuration;  $TT$  was smaller in people with epilepsy than controls in the PLI +  $d_S$  configuration (see Figure 2f). All other differences between the two groups were not statistically significant ( $p$ -values were corrected with the Bonferroni–Holm procedure). Finally, we repeated the same analysis using RPs with densities of recurrence points of 1% and 10% and found similar results. These results suggest that dFNs from people with epilepsy recur



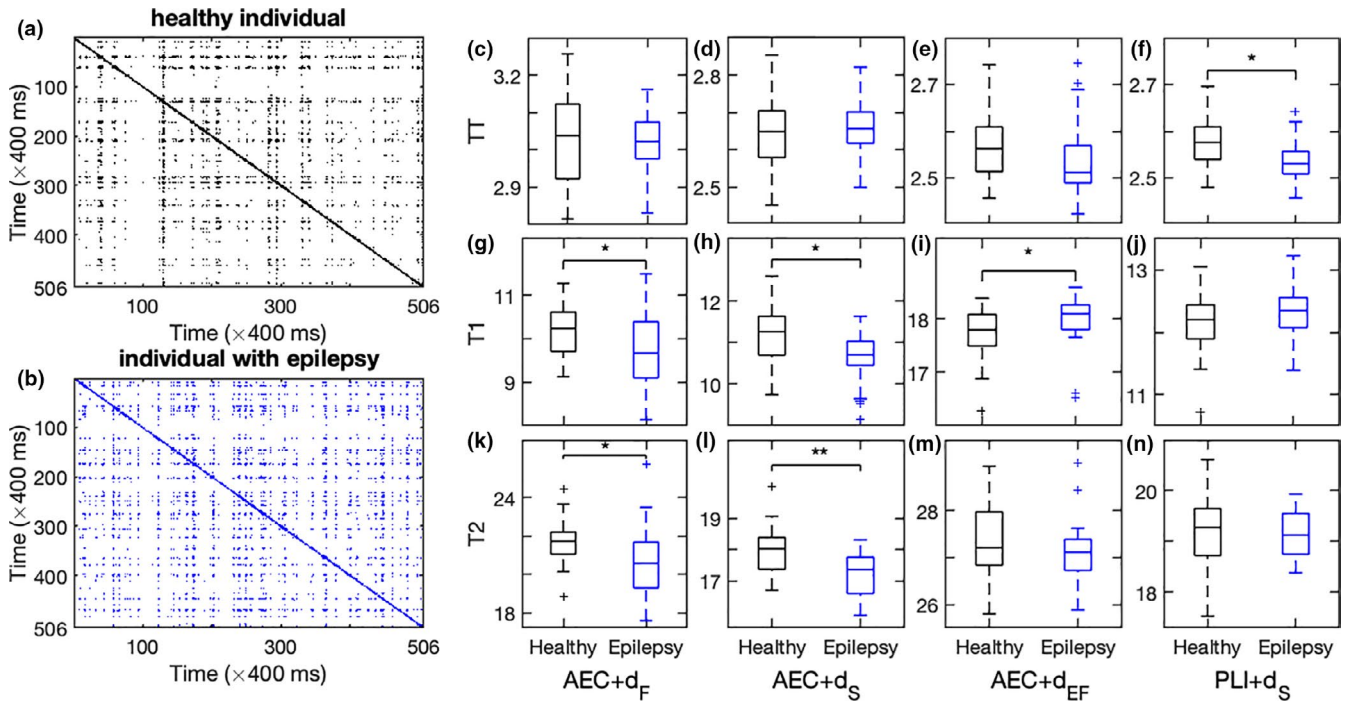


**FIGURE 2** Recurrence quantification analysis of dynamic MEG functional networks. (a) Representative RP from a healthy individual. (b) Representative RP from an individual with epilepsy. We used the AEC +  $d_F$  configuration. (c–f) Box plots of the trapping time ( $TT$ ) of the RPs from healthy controls and people with epilepsy. Each of the four panels in this row compares controls to people with epilepsy in one of the four configurations, i.e. AEC +  $d_F$ , AEC +  $d_S$ , AEC +  $d_{EF}$ , and PLI +  $d_S$ . Similarly, the rows of panels (g–j) and (k–n) show box plots for the recurrence time of first type ( $T1$ ) and second type ( $T2$ ), respectively, across the four configurations. In (f), (g), (h), (i), (k) and (l), significant differences between controls and people with epilepsy are indicated by asterisks (one asterisk represents  $p < .05$ , and two asterisks  $p < .01$ , Mann–Whitney  $U$  test, Bonferroni–Holm corrected). We used a density of recurrence points of 0.05 to define the threshold  $\in$

more often but are less likely to be trapped into specific FNs than dFNs from healthy people.

The group differences observed above suggest that RQA measures may be used to classify individuals as to whether they had epilepsy. To confirm and quantify the predictive power of RQA measures, we performed a classification analysis. First, we employed the  $T2$  measure to predict whether RPs from the AEC +  $d_S$  configuration were obtained from people with epilepsy or from healthy controls. Note that this was the combination of RQA measure and configuration for which the  $p$ -value was the smallest among all combinations of an RQA measure and configuration when comparing the epilepsy and healthy groups. We performed the receiver operating characteristic (ROC) analysis and found an AUC of 0.76, sensitivity of 0.58 and specificity of 0.88 (see Figure 3a). We then used MATLAB's Classification Learner Toolbox to classify the two groups using the  $T2$  values in the AEC +  $d_S$  configuration. We found an accuracy of 69.2% using a logistic regression, i.e. 36 out of 52 individuals were correctly classified (see the blue bar in Figure 3b). Next, we used the 11 RQA measures altogether and found that the classification accuracy was similar across the four configurations, ranging from 65.4% to 71.2% classification accuracy (see the black bars in Figure 3b). Finally, we tested

whether combining all RQA measures from the four configurations yielded a higher accuracy. To this end, as described in Section 2.7, to do it we first reduced the number of features by using PCA. We observed that the first 12 principal components explained 85% of the variance of all RQA measures and all configurations. Therefore, we used them to perform the classification. These principal components yielded a slightly lower accuracy to that for the other classification methods (see red bar in Figure 3b). Figure 3b shows the classification accuracy obtained from the best classifiers using MATLAB's Classification Learner Toolbox. The selected classifiers were the medium kNN for the AEC +  $d_S$  configuration, the cosine kNN for the AEC +  $d_{EF}$  configuration, the coarse tree for the AEC +  $d_F$  configuration and PCA and the fine kNN for the PLI +  $d_S$  configuration. Table S1 shows the classification accuracy obtained by each classifier employed by MATLAB's Classification Learner Toolbox.

We also performed the same classification analysis by (a) using the weighted mean degree of the functional networks and (b) by applying RQA to traditional RPs obtained from the MEG time series, rather than from the dFNs (see Supporting Information S7 and S8). We obtained a classification accuracy of 67.3% using the weighted mean degree and an accuracy of 69.2% using the traditional RQA analysis.

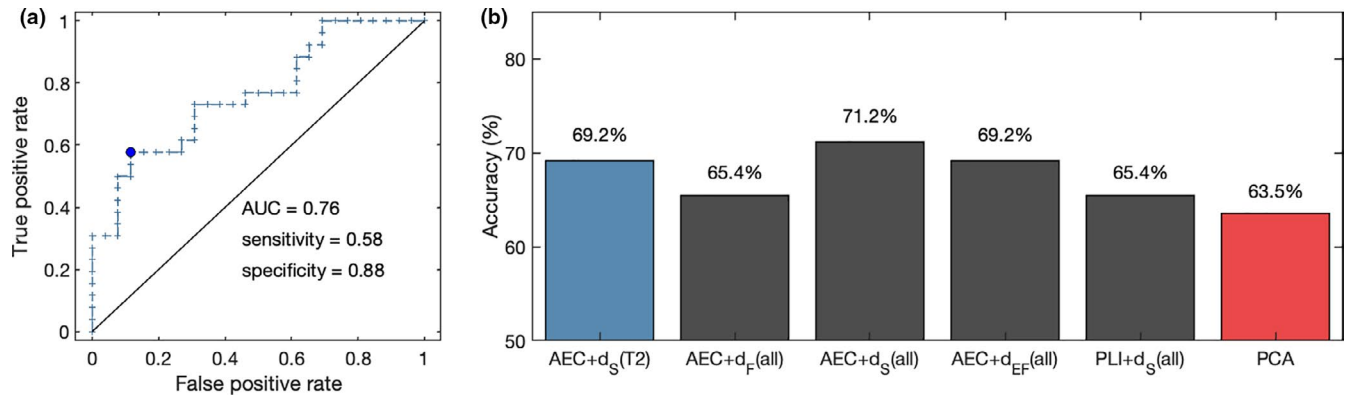


**FIGURE 3** Classification of people with epilepsy using RQA applied to dFNs inferred from MEG data. (a) Receiver operating characteristic (ROC) analysis to classify people as either healthy or with epilepsy using the recurrence time of second type ( $T_2$ ) from the configuration AEC +  $d_S$ . The circle represents the optimal operating point of the ROC curve, for which the sensitivity is equal to 0.58, and the specificity is equal to 0.88. The area under the curve (AUC) is equal to 0.76. (b) Accuracy of the classification using different features from the RQA analysis and 50-fold cross-validation: the recurrence time of second type ( $T_2$ ) from the AEC +  $d_S$  configuration (blue bar), all RQA measures from each of the four representative configurations (grey bars), and 12 principal components explaining 85% of the variance of all RQA measures across the four configurations (red bar)

### 3.2 | Dynamic sEEG functional networks

We also applied our framework to dFNs inferred from sEEG data from people with drug-resistant focal epilepsy. In contrast to the resting-state MEG data, the sEEG data contained electrographic seizures. Here our purpose was to observe how dFNs change upon seizure onset and offset, whether dFNs are consistent across different seizures and whether seizure onset may be identifiable using our framework.

We considered one broad frequency band, the Pearson's correlation as connectivity measure, and the same six distance measures between functional networks as in the study of the MEG data set. As a result of applying the reduction of configurations (see Supporting Information S5), we focused our analysis on three distance measures:  $d_F$ ,  $d_S$  and  $d_{EF}$ .

We analysed sEEG data from 10 individuals, each of them with two to four peri-ictal epochs. There were 29 peri-ictal epochs in total. Each peri-ictal epoch contained five minutes of data before seizure onset (pre-ictal), the seizure (ictal) and five minutes of data after seizure offset (post-ictal). Our aim was to observe whether functional networks show stereotypical dynamics throughout seizures, whether we can detect seizures and how the pre-ictal, ictal and post-ictal networks relate to each other.

For each peri-ictal epoch of each individual, we computed a sequence of  $M$  functional networks using Pearson's correlation, where  $M$  varied between 1542 and 1822 with median 1632, depending on the length of the ictal periods. Below, we present results obtained using the Frobenius norm, Equation (3), to compute the distance between functional networks, and using a threshold such that the RPs had a density of recurrence points equal to 0.05. We obtained similar results using the two other distance measures and using the two other

threshold values (i.e. thresholds such that the RPs had a density of recurrence points equal to 0.01 and 0.1).

#### 3.2.1 | RPs of multiple peri-ictal epochs

To assess whether similar functional networks are involved in different pre-ictal, ictal and post-ictal epochs from different peri-ictal epochs of an individual, we first concatenated the sequences of functional networks from different peri-ictal epochs of the individual. Next, we computed the distance between each pair of networks in the concatenated sequence to obtain a distance matrix (see Figure 1c). Then, by thresholding the distance matrix, we obtained an RP (see Figure 1d). Figure 4a,b show RPs for two individuals. Each RP contains three peri-ictal epochs. We observe that most of the recurrence points are located in the pre-ictal periods (i.e. in the first, fourth and seventh diagonal blocks) and that there is also a high density of recurrence points in off-diagonal blocks corresponding to the cross relation between different pre-ictal periods. The ictal periods also show high density of recurrence points within the same peri-ictal epoch and between different peri-ictal epochs. In contrast, the post-ictal periods show a low density of recurrence points both within and between epochs. These results imply that pre-ictal and ictal functional networks are more similar between themselves than post-ictal functional networks. There is also a considerable frequency of recurrence between pre-ictal and ictal networks, both within and between epochs. This result suggests that the functional networks involved in seizures emerge before seizure onset. In contrast, the functional networks after seizure offset are relatively different from networks during both pre-ictal and ictal periods.

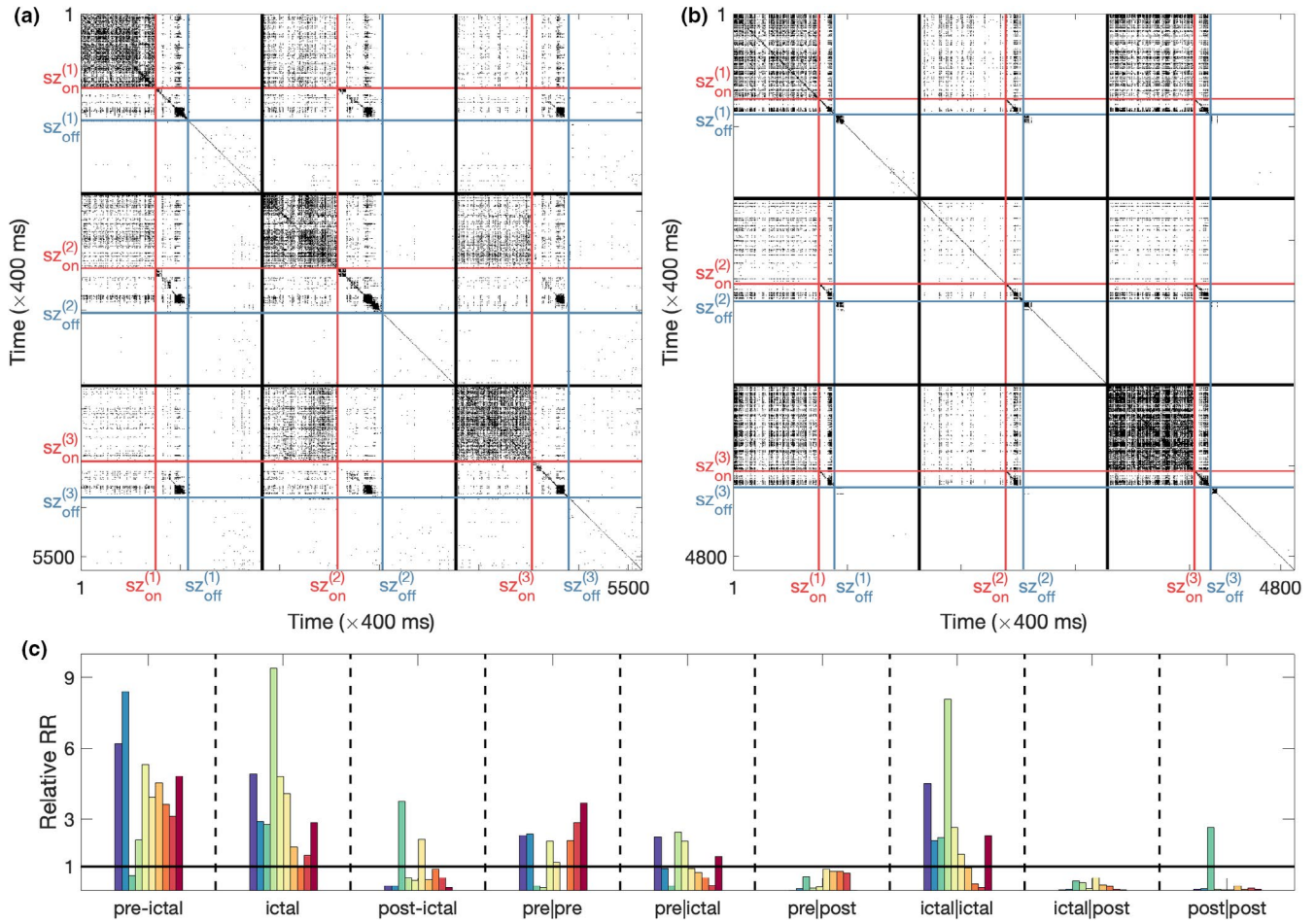


**FIGURE 4** Recurrence plots (RPs) and relative recurrence rate (*RR*) of sEEG dFNs from individuals with epilepsy. (a) RP for three peri-ictal epochs of one individual. The thick black lines separate the three peri-ictal epochs. The thin red and blue lines indicate the seizure onset and offset in each peri-ictal epoch respectively. Panel (b) is equivalent to (a) but for a different individual. (c) Relative *RR* for all individuals with epilepsy. For each individual, we consider the relative *RR* in nine types of blocks in the RPs: the label ‘pre-ictal’ corresponds to the three pre-ictal diagonal blocks of the RP; ‘ictal’ corresponds to the three ictal diagonal blocks; ‘post-ictal’ corresponds to the three post-ictal diagonal blocks; ‘pre|pre’ corresponds to the six off-diagonal blocks that compare different pre-ictal periods; ‘pre|ictal’ corresponds to the 18 off-diagonal blocks that compare pre-ictal and ictal periods; ‘pre|post’ corresponds to the 18 off-diagonal blocks that compare pre-ictal and post-ictal periods; ‘ictal|ictal’ corresponds to the six off-diagonal blocks that compare different ictal periods; ‘ictal|post’ corresponds to the 18 off-diagonal blocks that compare ictal and post-ictal periods; and the ‘post|post’ corresponds to the six off-diagonal blocks that compare different post-ictal periods. For each type of block, we plot 10 bars, one for each individual. The two leftmost bars correspond to the RPs shown in (a) and (b) respectively. The chance level, i.e. 1, is represented by the solid horizontal line. Figure S2 shows that the results in (c) remain similar for other configurations (i.e. using different distance measures between networks)

To quantify the observations made from Figure 4a,b, we measured the relative recurrence rate (*RR*) defined as the fraction of the actual recurrence points in a block divided by the fraction of recurrence points expected by chance, i.e. 5% (because the overall density of recurrence points was set to 5%). Figure 4c shows the relative *RR* of each type of block in the RPs for all individuals. The two leftmost bars in each type of block in Figure 4c correspond to the two individuals whose RPs are shown in Figure 4a,b and confirm our previous observations. The relative *RR* of these two individuals further shows that, whereas the recurrence rate between a pre-ictal period and an ictal period belonging to different peri-ictal epochs is not higher than chance in Figure 4a, it is higher than chance

in Figure 4b. Overall, Figure 4c shows that the pre-ictal periods have recurrence rates higher than chance in nine out of the 10 individuals. The ictal periods also have higher recurrence rates than chance in all but one individual. Post-ictal periods have low recurrence rates, except in two individuals. The cross relations between different pre-ictal periods, between pre-ictal and ictal periods and between ictal periods show considerable variability in terms of the relative *RR*, which is either below or above chance depending on the individual. In contrast, the cross relations between pre-ictal and post-ictal periods, between ictal and post-ictal periods and between different post-ictal periods are consistently lower than chance, except in one individual that has high relative *RR* in the cross relation between different



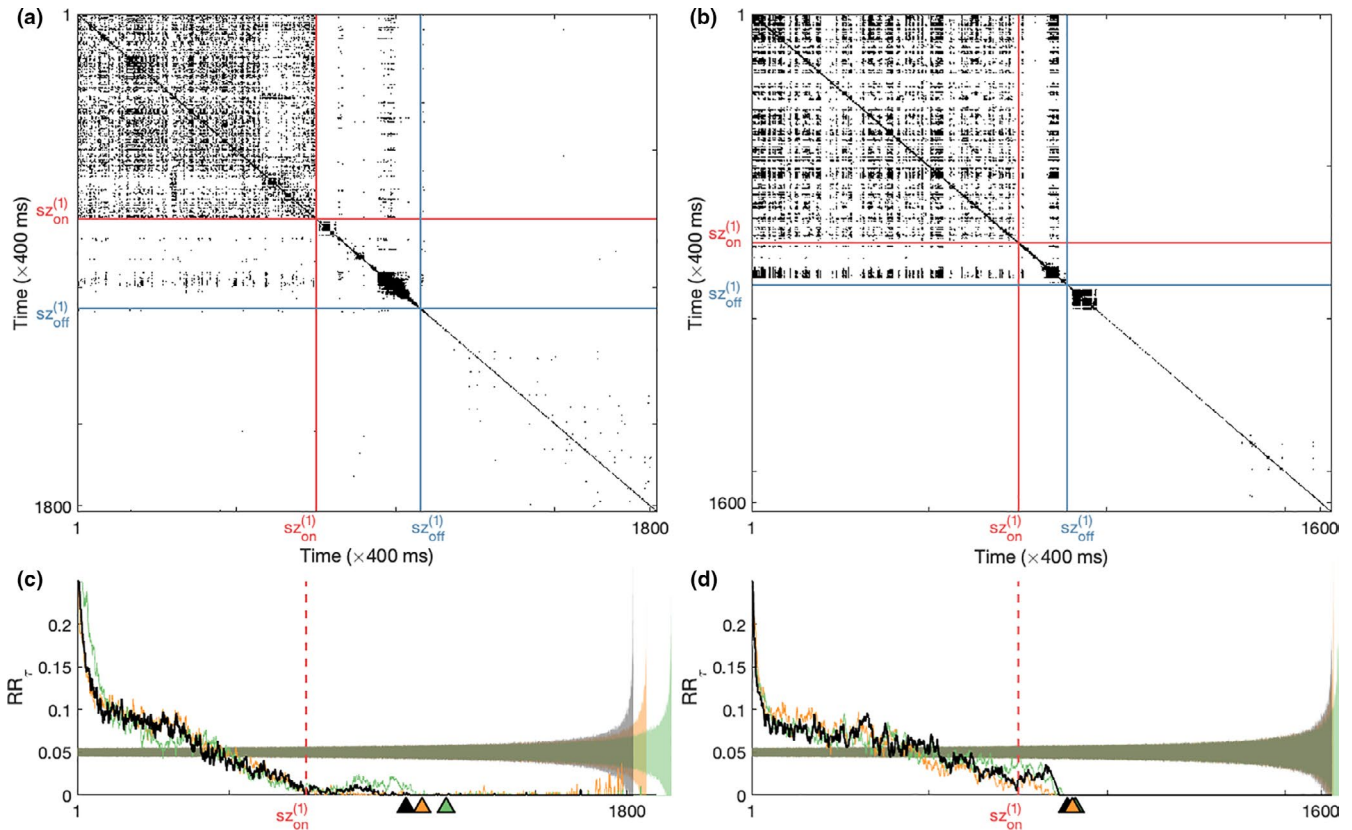


**FIGURE 5** Recurrence plots (RPs) and  $\tau$ -recurrence rate ( $RR_\tau$ ) of sEEG dFNs during single peri-ictal epochs. (a) RP of dFNs during one peri-ictal epoch of one individual with epilepsy. This peri-ictal epoch corresponds to the first peri-ictal epoch shown in Figure 4a. The seizure onset and offset are indicated by the red and blue lines, respectively. (b) Same as (a) but for a peri-ictal epoch of a different individual, i.e. the first peri-ictal epoch in Figure 4b. (c)  $RR_\tau$  for three peri-ictal epochs for the individual considered in (a). (d) Same as (c) but for the RP shown in (b). In (c) and (d), the black line represents the  $RR_\tau$  computed from the RP in (a) and (b), respectively; the other two lines correspond to the other two peri-ictal epochs of the same individual; the dashed lines indicate time lags equal to the time of seizure onset for all peri-ictal epochs; the triangles indicate time lags equal to the time of seizure offset, where the colour of the triangle matches that of the  $RR_\tau$  curve. The shaded areas represent the standard deviation of  $RR_\tau^{null}$  above and below its mean obtained from 100 random shuffles of the RPs of each peri-ictal epoch. At large  $\tau$ , the standard deviation of  $RR_\tau^{null}$  increases, because the diagonal lines at large  $\tau$  in the RP matrix have fewer elements, i.e.  $M - \tau$  elements. Therefore, for large  $\tau$ ,  $RR_\tau$  is highly quantized; it can take values  $0, 1/(M - \tau), 2/(M - \tau), \dots, 1$  (see Equation 6), resulting in a large statistical fluctuation in  $RR_\tau$ .

post-ictal periods. These results support that the observations made from Figure 4a,b for two individuals generalize to most of the 10 individuals. The individual represented by the third bar from the left in Figure 4c (shown in dark green) is an outlier.

To test whether these results were confounded by the different number of peri-ictal epochs per individual, we further computed the relative  $RR$  using only two peri-ictal epochs from each individual. For individuals with more than two peri-ictal epochs, we computed the relative  $RR$  for all combinations of two peri-ictal epochs. Figure S3 shows the result of this analysis. We observe that the results in Figure S3 are similar to those in Figure 4c, meaning that most combinations of two peri-ictal epochs from each individual produce approximately the same relative  $RR$  pattern as that produced by all peri-ictal epochs combined together. Thus, these results suggest that the results in Figure 4c are not confounded by the number of peri-ictal epochs of each individual.

### 3.2.2 | RPs of single peri-ictal epochs

We then assessed whether or not RQA may be able to detect seizures. RPs comprising multiple peri-ictal epochs are not appropriate for this purpose, because a peri-ictal epoch may have a disproportionately high or low fraction of recurrence points compared to other peri-ictal epochs for the same individual. Therefore, here we did not concatenate the sequences of functional networks over different peri-ictal epochs. Instead, we constructed an RP for each of the 29 peri-ictal epochs.

Figure 5a,b show RPs from a peri-ictal epoch of different individuals. These figures show that the pre-ictal periods present a higher recurrence rate than both ictal and post-ictal periods, in agreement with Figure 4. Transitions in the RPs are also noticeable at the seizure onsets. Furthermore, whereas there is recurrence of pre-ictal networks in the ictal



period, there is neither recurrence of pre-ictal nor ictal networks in the post-ictal period. Additionally, the post-ictal period has a small number of recurrence points.

To assess the potential of RQA to detect seizure onset, we computed the  $\tau$ -recurrence rate ( $RR_\tau$ ) for the RPs shown in Figure 5a,b. The  $\tau$ -recurrence rate quantifies the frequency of recurrence when pairs of functional networks are  $\tau$  time points apart. When  $\tau$  is larger than the seizure onset time,  $RR_\tau$  measures recurrences of pre-ictal networks in the ictal and post-ictal periods, as well as recurrences of ictal networks in the post-ictal period. When  $\tau$  is larger than the seizure offset time,  $RR_\tau$  only uses recurrences of pre-ictal networks in the post-ictal period. In contrast, when  $\tau$  is smaller than the seizure onset time,  $RR_\tau$  also accounts for recurrences within the pre-ictal period and within the post-ictal period, as well as within the ictal period when  $\tau$  is also smaller than the duration of the seizure. Because the relative  $RR$  is large in the pre-ictal period, but small in the cross relation between pre- and post-ictal periods, we expect that  $RR_\tau$  is large if and only if  $\tau$  is smaller than the seizure onset time. Furthermore, we expect that  $RR_\tau$  decreases as  $\tau$  increases from zero towards the seizure onset time because the contribution of

recurrences within the pre-ictal period to  $RR_\tau$  decreases as  $\tau$  increases in this range. Therefore,  $RR_\tau$  may be a useful tool for detecting seizure onset.

The  $\tau$ -recurrence values for the two individuals are shown in Figure 5c,d. As anticipated, the  $RR_\tau$  decreases towards 0 as  $\tau$  approaches the value corresponding to the seizure onset time in Figure 5c and corresponding to the seizure offset time in Figure 5d. For both individuals,  $RR_\tau$  remains near zero for larger  $\tau$  values. The difference between the two individuals results from the fact that pre-ictal networks do not often recur in the ictal period for the individual represented in Figure 5a,c, but they do recur for the individual represented in Figure 5b,d. Figure 5c,d also display the results for other peri-ictal epochs from the same individuals, confirming qualitatively the same observations. We also plotted the mean and standard deviation of  $RR_\tau^{\text{null}}$  above and below its mean as the shaded regions, which represents a distribution of  $RR_\tau$  obtained from randomized RPs. The mean of  $RR_\tau^{\text{null}}$  is 0.05 for any  $\tau$ , which is the density of recurrence points in the RP. This is because, in a randomized RP, every diagonal line, corresponding to a value of  $\tau$ , has on average the same density of

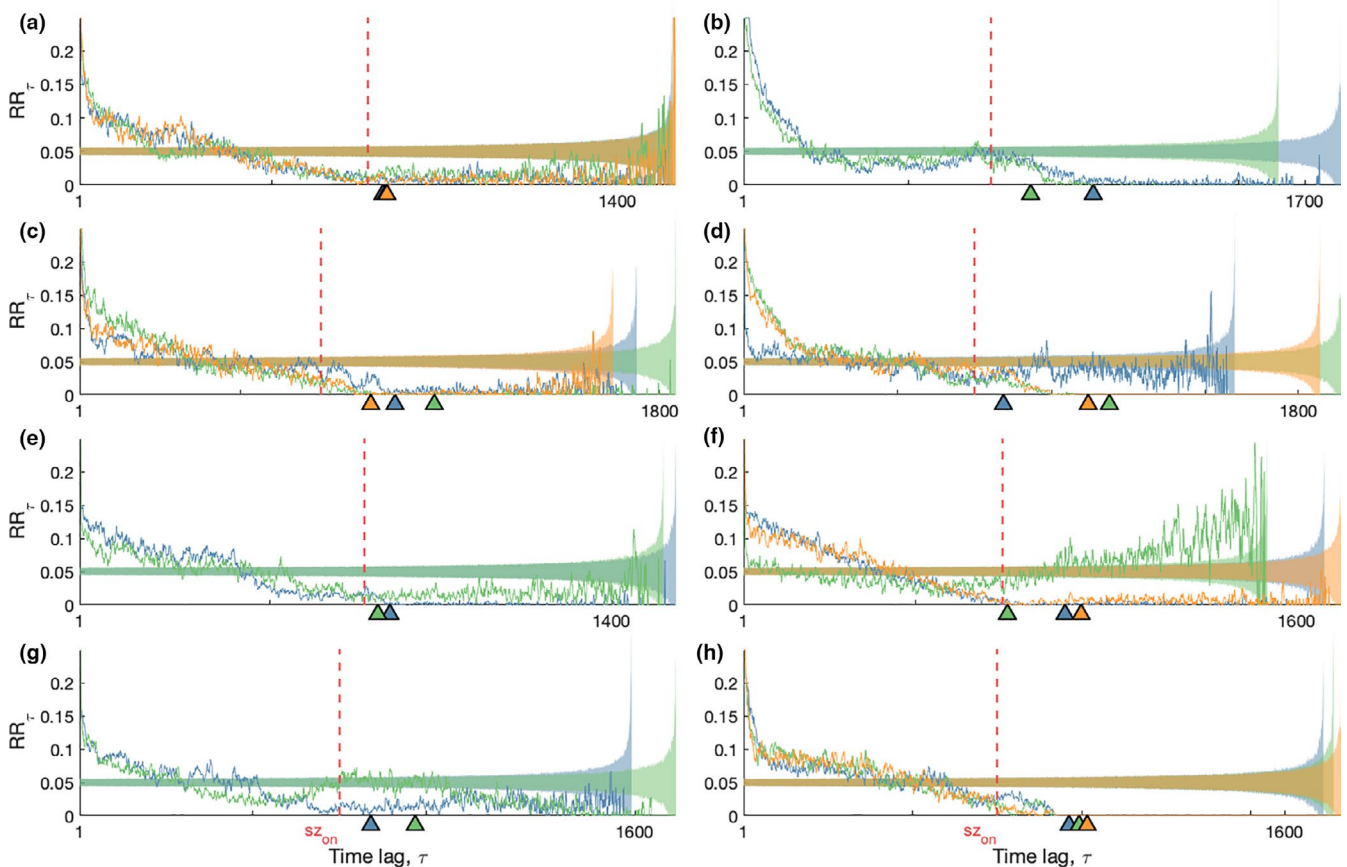


**FIGURE 6**  $\tau$ -recurrence rate ( $RR_\tau$ ) of sEEG dFNs during single peri-ictal epochs for eight individuals. Each panel represents a different individual. Each individual had between 2 and 4 peri-ictal epochs, which are represented as lines in different colours. The dashed lines indicate the time lag equal to the time of seizure onset. The coloured triangles indicate the time lag equal to the time of seizure offset of the  $RR_\tau$  curve in the same colour. The shaded areas represent the standard deviation of  $RR_\tau^{\text{null}}$  above and below its mean obtained from 100 random shuffles of the RPs of each peri-ictal epoch

points as the original RP. Figure 5c,d indicate that  $RR_\tau$  is significantly larger than for the randomized RPs when  $\tau$  is small and that it is significantly closer to zero than the randomized RPs as  $\tau$  becomes large and approaches the seizure onset.

We performed the same analysis for the other eight individuals and found that  $RR_\tau$  decreases to values close to zero at seizure onset or close to seizure offset in the majority of the peri-ictal epochs considered (see Figure 6). There are three notable exceptions (the blue line in Figure 6d, and the green lines in Figure 6f,g), which do not show a decrease in  $RR_\tau$  at either seizure onset or offset. Overall, the results suggest that a decrease in  $RR_\tau$  to values close to zero at a certain  $\tau$  value is indicative of a seizure onset or offset at time  $\tau$ .

### 3.2.3 | RPs of individual pre- and post-ictal periods

We have shown that the recurrence rate within the pre-ictal period is much higher than within the post-ictal period (see Figure 4c). An RP for a peri-ictal epoch, which by definition contains a pre-ictal, ictal and post-ictal period altogether (e.g. Figure 5), does not allow us to compare recurrence features of functional networks within the pre-ictal period to those within the post-ictal period due to the difference in density of recurrence points in the two periods. To address this limitation, and to compare the dynamics of functional networks between pre-ictal and post-ictal epochs, we constructed RPs containing only a pre-ictal or a post-ictal period. We did not consider RPs only containing an ictal period because the ictal periods were typically too short for RQA. Figure 7a,b show an RP from a pre-ictal and post-ictal period, respectively, belonging to the same peri-ictal epoch. By construction, the two RPs had the same recurrence rate, which allowed us to compare other properties of the RPs between the pre-ictal and post-ictal periods.

Figure 7c–e show the variation of  $DET$ ,  $L$  and  $L_{max}$  between all pre- and post-ictal RPs within the same peri-ictal epoch for all individuals. We observe that in most peri-ictal epochs these three measures are larger in the post-ictal than pre-ictal periods (i.e. positive variation values), meaning that post-ictal RPs have typically longer diagonal lines than pre-ictal RPs. We used the Wilcoxon signed-rank test to assess the significance of these changes and found  $\Delta DET$  and  $\Delta L_{max}$  significant and  $\Delta L$  at the boundary of significance. This result suggests that post-ictal dFNs may be more deterministic than pre-ictal dFNs. For some individuals, this variation is consistently positive (i.e. the post-ictal values are larger than the pre-ictal values) for all their peri-ictal epochs (e.g. the individual represented by the right-most triangles in Figure 7c–e).

Figure S4 shows the variation of the other RQA measures. The  $ENTR$ ,  $LAM$ ,  $TT$ ,  $V_{max}$  and  $Trans$  values tended to be

larger in the post-ictal than pre-ictal periods, whereas the opposite was the case for  $T1$ ,  $T2$  and  $RT E$ . The measures based on vertical lines ( $LAM$ ,  $TT$  and  $V_{max}$ ) indicate that dFNs are more likely to be trapped in slowly changing functional networks in the post-ictal than the pre-ictal period.

## 4 | DISCUSSION

In this study, we have proposed to use RPs and RQA to study dFNs. The framework consists of assessing the distance between functional networks at different times and define recurrences if the distance is within a threshold. By doing so, one obtains an RP on which one can perform RQA. The RQA measures inform us about the underlying dynamics of the functional networks. We applied this framework to two data sets, (a) resting-state MEG recordings from people with JME and healthy controls, and (b) sEEG recordings containing peri-ictal epochs of people with drug-resistant focal epilepsy undergoing pre-surgical evaluation. The purpose of these two independent analyses was to show the broad applicability of the framework and its potential to address a wide range of hypotheses. In the MEG data set, we found that RQA measures for dynamic resting-state functional networks differed between people with epilepsy and healthy controls. In the sEEG data set, we found that pre-ictal functional networks show high recurrence not only within pre-ictal periods but also between different pre-ictal periods, and that they also recur during ictal periods. This result implies not only that functional networks involved in seizures emerge before seizure onset, but also that they are consistent across different seizures. We also observed that RQA measures were capable of detecting seizures. Finally, we observed that post-ictal dFNs are typically more deterministic and more likely to be trapped into certain networks compared to pre-ictal dFNs.

Using the MEG data set, we found significantly smaller recurrence time in people with epilepsy compared to healthy controls (for both first ( $T1$ ) and second type ( $T2$ ) and in both the  $AEC + d_F$  and  $AEC + d_S$  configurations; see Figure 2g,h,k,l). This result implies that AEC functional networks recur more quickly in people with epilepsy than in controls. This finding suggests that the space of possible functional networks may be more limited in epilepsy. We speculate that a reduced repertoire of functional networks may lead to functional brain deficits. This is in agreement with the fact that cognitive deficits are commonly observed in people with epilepsy (Holmes, 2015). Future work should test the hypothesis that reduced recurrence times predict cognitive deficits. One should also further examine such findings across different configurations (see Supporting Information S9).

We then used RQA measures to classify people as to whether they had epilepsy and found an accuracy of 71.2% (see Figure 3). This classification power is similar to that

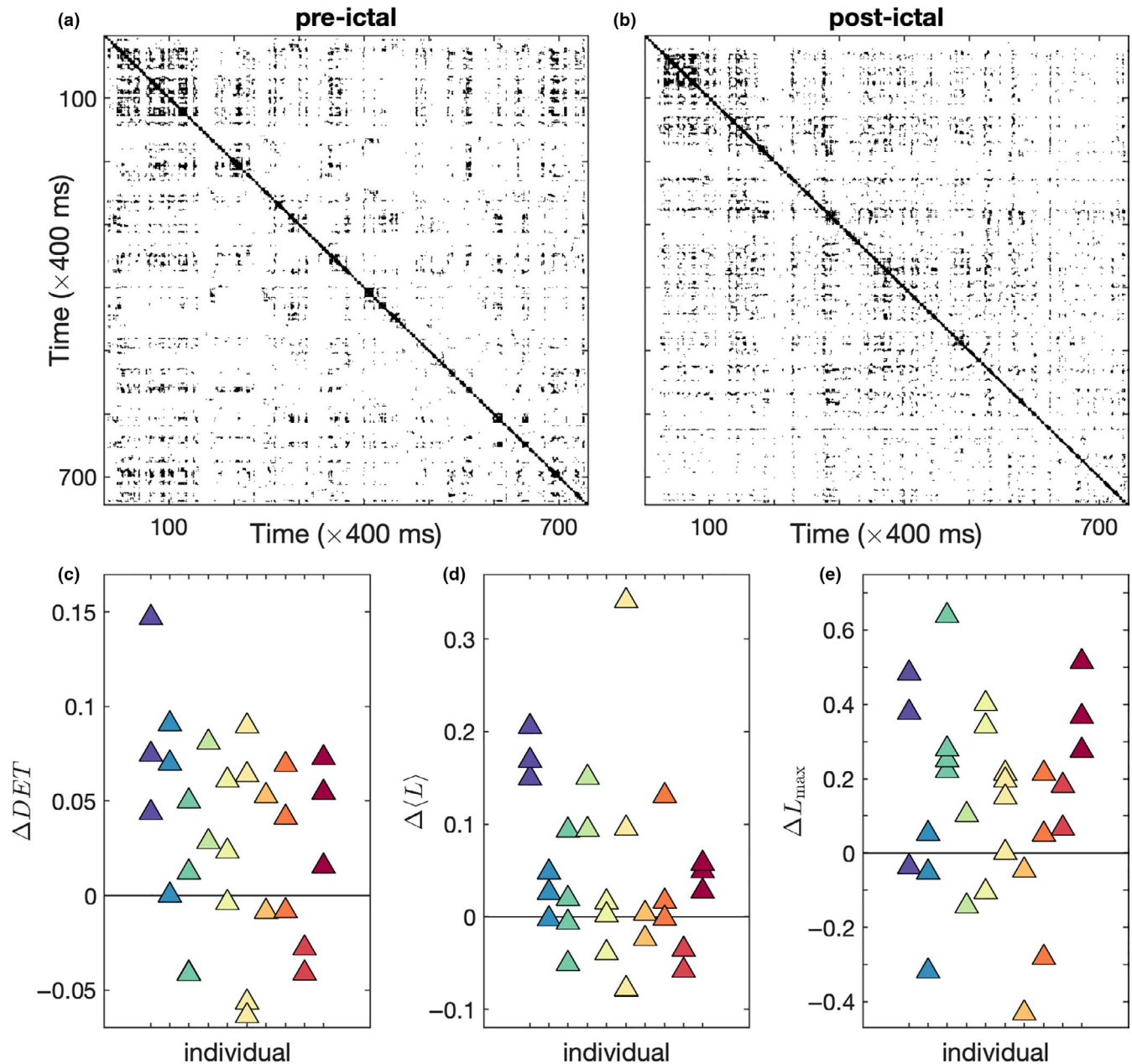


**FIGURE 7** Comparison between pre- and post-ictal recurrence plots (RPs) of sEEG dFNs. (a) RP of dFNs during a pre-ictal period of one individual with epilepsy. (b) RP of dFNs during a post-ictal period corresponding to the same individual and the same peri-ictal epoch as in panel (a). Panels (c), (d), and (e) show the  $DET$ ,  $L$ , and  $L_{max}$  variation, respectively, between pre- and post-ictal RPs. Wilcoxon signed-rank tests showed that  $DET$  and  $L_{max}$  significantly changed from pre- to post-ictal epochs, and the variation of  $L$  was at the boundary of significance (the  $p$ -values were .01 for  $\Delta DET$  and  $\Delta L_{max}$ , and 0.05 for  $\Delta L$ ). A triangle corresponds to a peri-ictal epoch. The colour of the triangles as well as their horizontal positions distinguishes the individuals

achieved with single resting-state scalp EEG functional networks for people with idiopathic generalized epilepsy (Schmidt et al., 2016). In our study, we considered juvenile myoclonic epilepsy, which is a specific type of generalized epilepsy. Future work should test whether our findings extend to other types of both generalized and focal epilepsy. Furthermore, drug-naïve individuals should be recruited in order to exclude the possibility that the differentiation between people with epilepsy and healthy controls is due to

medication intake, and not epilepsy. Notably, the opportunity to use resting-state data to distinguish people with epilepsy from healthy people is of great clinical value because current clinical practice depends upon the observation of epileptiform discharges which are not always apparent in a scalp EEG session (Smith, 2005). As scalp EEG is more inexpensive and available than MEG, future work should also test whether our findings generalize to dFNs inferred from scalp EEG.

We also assessed whether the combination of our approach with others achieved a superior classification accuracy. The mean number of connections in EEG functional networks has been used to differentiate between people with idiopathic generalized epilepsy and controls (Chowdhury et al., 2014). Therefore, we computed the weighted mean degree of our MEG functional networks and used it to classify the individuals (see Supporting Information S7). We obtained 67.3% accuracy, which was slightly lower than the classification accuracy that we attained with the RQA measures on dFNs. The accuracy did not improve by combining the weighted mean degree with the RQA measures. Additionally, we also used traditional RQA measures applied to RPs obtained from the MEG time series to classify the individuals (see Supporting Information S8). We found an accuracy of 69.2%, i.e. similar to the accuracy achieved using the RQA for dFNs. Again, we found that combining the two types of RQA did not improve the accuracy of the classification. This result suggests that the two types of analysis may extract similar information. However, this does not imply that the two methods are equivalent. By inferring dFNs and studying their recurrences, we are examining the recurrences of statistical dependencies between the MEG signals. In contrast, the traditional recurrence analysis looks at the recurrence of the MEG signals themselves. Another difference between the two methods is that by computing dFNs we reduced the time resolution of the recurrence analysis, i.e. from 4 ms in the traditional RPs to 400 ms in our RPs. Future work should further explore the relation between the two methods and test whether they may complement each other on various data sets.

We highlight that our analysis in the MEG data set was based on functional networks inferred in the theta band, and that their recurrence was representative of the recurrence of dFNs in other frequency bands (see Supporting Information S5). This is an unexpected result given that MEG functional networks are usually different across different frequency bands (Tewarie et al., 2016). Notwithstanding, our results suggest that the recurrence of dFNs, at least using measures afforded by RQA, may be similar across frequency bands. Further investigation of the recurrence of dFNs in different frequency bands is needed to ascertain their cross-frequency relations.

Using the sEEG data set, we found considerable recurrence of pre-ictal and ictal functional networks in their respective periods (see Figure 4c). We further observed that ictal functional networks recurred in different seizures for most of the individuals, and that there was considerable recurrence of functional networks between different pre-ictal periods and between pre-ictal and ictal periods. Such information may be useful when evaluating whether there are one or more leading networks that sustain seizures. Non-recurrence of functional networks across different seizures may be a contraindication for epilepsy surgery because multiple seizure focus may be

involved. In contrast, functional networks that recur both in pre-ictal and ictal periods across different peri-ictal epochs may support epilepsy surgery and they may be used to inform where to perform the resection (Goodfellow et al., 2016; Kini et al., 2019; Lopes et al., 2017, 2018). Future work should test whether the combination of our framework with other recent methods that use functional networks to inform epilepsy surgery and predict surgery outcome (Goodfellow et al., 2016; Kini et al., 2019; Lopes et al., 2017, 2018) yield superior predictions.

Seizure detection is highly relevant not only for seizure management (Jory et al., 2016), but also to assist neurologists in the analysis of EEG (Adeli, Zhou, & Dadmehr, 2003). We observed that the  $\tau$ -recurrence rate ( $RR_\tau$ ) values decreased to close to zero when  $\tau$  approached the seizure onset or offset time in peri-ictal epochs from all individuals, except for three peri-ictal epochs (see Figures 5c,d and 6).  $RR_\tau$  takes advantage of the fact that functional networks frequently recur within the pre-ictal period and relatively rarely within the post-ictal period. These findings suggest that our framework may be useful for seizure detection. Future work should assess whether the decrease in  $RR_\tau$  is specific to seizures, which one can assess by additionally measuring  $RR_\tau$  far from seizures (i.e. in the inter-ictal periods, which we did not consider in this study because of lack of such data). In such future work, one should consider assessing  $RR_\tau$  not relative to randomly shuffled RPs as we did in Figures 5c,d and 6, but rather relative to an inter-ictal baseline. Additionally, our methods should be compared to other recent methods to detect seizures (Leijten et al., 2018). Beyond sEEG data, it should be tested whether this method may be useful for seizure detection from scalp EEG.

We also found that the dynamics of functional networks tended to be more deterministic and more frequently trapped in certain functional networks in the post-ictal period than in the pre-ictal period (see Figure 7; Figure S4). We hypothesize that individuals who show consistent differences in RQA measures between pre-ictal and post-ictal periods across seizures may be particularly suited to receiving neurostimulation treatment (Morrell, 2006). Neurostimulation can be used to modulate brain activity of people with epilepsy to avoid the emergence of seizures (Morrell, 2006). Thus, we suggest that our framework may be used for finding whether an individual presents differences in dFNs between the pre-ictal and post-ictal periods that are consistent across seizures. Such a consistency supports the use of a single stimulation strategy that may be reliable across peri-ictal epochs. Furthermore, our framework also informs us of the specific differences between pre-ictal and post-ictal dFNs. A personalized stimulation strategy may then be designed such that it modulates the dynamics of pre-ictal functional networks into those of the post-ictal period, thereby avoiding seizures (Dalkilic, 2017).

There are a number of confounding factors to consider when assessing our sEEG results. First and foremost, each individual



had different causes of epilepsy with seizures emerging from different brain regions and each individual received different electrode implantations. Consequently, functional networks from different individuals had different numbers of nodes (i.e. channels) and covered different regions of the brain. Such differences may account for some of the variability observed among individuals. Second, even for the same individual, different peri-ictal epochs contained seizures of varying lengths, and peri-ictal epochs were at different time distances from other seizures. The distance to other seizures may be an important confounding factor when comparing pre-ictal and post-ictal periods. Third, although we used 5 min before and after a seizure as a pre-ictal and post-ictal period, respectively, this choice was motivated by the need for a sufficient number of functional networks for our analysis, rather than a clinically motivated decision. Different definitions of pre-ictal and post-ictal periods may yield different results.

Although we applied our framework to dFNs inferred from MEG and sEEG data, in principle the framework is applicable to any kind of time-varying network or matrix. An important requirement is to have a sufficient number of networks or matrices to reliably evaluate their dynamics and recurrences (Marwan et al., 2007). Thus, the framework may not be applicable to study dFNs derived from typical fMRI experiments due to a relatively small number of time points (Hutchison et al., 2013). For this reason, we did not explore the dynamics of functional networks during seizures in the sEEG data set; seizures were not long enough for our analysis. Additionally, although we focused on epilepsy in this study, our framework may also be suitable to studying healthy brain function or other brain disorders.

There are other computational approaches to dFNs. Common approaches include tracking certain network measures over time (Sizemore & Bassett, 2018), using hidden Markov models (Eavani et al., 2013; Sourty et al., 2016; Vidaurre et al., 2018), and considering dynamic networks as multilayer networks (De Domenico et al., 2013; Kivela et al., 2014; Sizemore & Bassett, 2018). Other recent approaches have used distance matrices to evaluate dFNs from fMRI (Cabral et al., 2017) and dynamic correlation matrices from scalp EEG (Rosch, Baldeweg, Moeller, & Baier, 2018). Future work should compare these different methods to our framework to find which one better characterizes dFNs in epilepsy and other contexts, and assess whether these approaches complement each other.

In conclusion, we propose a new framework to assess dFNs based on recurrence analysis. We applied the framework to source-localized resting-state MEG data and found that it is capable of distinguishing people with epilepsy from healthy controls. We also used the framework to assess sEEG dFNs and found supporting evidence that it may be useful for seizure detection. The framework further opens avenues to test new hypotheses, namely, to advance methods of epilepsy surgery assessment, and to potentially inform neurostimulation

strategies. The framework may also be used to study dFNs in healthy brain functions and in other neurological disorders.

## ACKNOWLEDGEMENTS

ML, JZ, LL and NM gratefully acknowledge funding from the GW4 Accelerator Fund. JZ further acknowledges the financial support from the European Research Council [grant number 716321]. DK was supported by an EPSRC PhD studentship [grant number EP/N509449/1]. KH acknowledges support from the Health and Care Research Wales: Clinical Research Time Award and the Wales BRAIN Unit. QC is supported by grants from the Natural Science Foundation of China (31871138), and by the Chang Jiang Scholars Program (2016). LL gratefully acknowledges partial support from the Canada Research Chairs program. NM acknowledges support from AFOSR European Office [grant number FA9550-19-1-7024].

## CONFLICT OF INTEREST

None.

## AUTHOR CONTRIBUTIONS

Marinho A. Lopes: Conceptualization; Methodology; Software; Formal analysis; Writing - Original Draft; Writing - Review & Editing; Visualization. Jiaxiang Zhang: Conceptualization; Writing - Review & Editing; Project administration; Funding acquisition. Dominik Krzemiński: Software; Formal analysis; Writing - Review & Editing. Khalid Hamandi: Investigation; Data Curation; Writing - Review & Editing. Qi Chen: Investigation; Data Curation; Writing - Review & Editing. Lorenzo Livi: Conceptualization; Methodology; Writing - Review & Editing; Funding acquisition. Naoki Masuda: Conceptualization; Methodology; Writing - Original Draft; Writing - Review & Editing; Supervision; Project administration; Funding acquisition.

## PEER REVIEW

The peer review history for this article is available at <https://publons.com/publon/10.1111/ejn.14960>

## DATA AVAILABILITY STATEMENT

All materials (functional networks and code) are available upon request (contact [m.lopes@exeter.ac.uk](mailto:m.lopes@exeter.ac.uk)).

## ORCID

Marinho A. Lopes  <https://orcid.org/0000-0002-5764-2261>

## REFERENCES

- Adeli, H., Zhou, Z., & Dadmehr, N. (2003). Analysis of EEG records in an epileptic patient using wavelet transform. *Journal of Neuroscience Methods*, 123(1), 69–87. [https://doi.org/10.1016/S0165-0270\(02\)00340-0](https://doi.org/10.1016/S0165-0270(02)00340-0)
- Bassett, D. S., & Sporns, O. (2017). Network neuroscience. *Nature Neuroscience*, 20(3), 353–364. <https://doi.org/10.1038/nn.4502>

- Bastos, A. M., & Schoffelen, J. M. (2016). A tutorial review of functional connectivity analysis methods and their interpretational pitfalls. *Frontiers in Systems Neuroscience*, *9*, 175. <https://doi.org/10.3389/fnsys.2015.00175>
- Braun, U., Schaefer, A., Betzel, R. F., Tost, H., Meyer-Lindenberg, A., & Bassett, D. S. (2018). From maps to multi-dimensional network mechanisms of mental disorders. *Neuron*, *97*(1), 14–31. <https://doi.org/10.1016/j.neuron.2017.11.007>
- Bullmore, E., & Sporns, O. (2009). Complex brain networks: Graph theoretical analysis of structural and functional systems. *Nature Reviews Neuroscience*, *10*(3), 186–198. <https://doi.org/10.1038/nrn2575>
- Buzsáki, G. (2006). *Rhythms of the brain*. Oxford: Oxford University Press.
- Cabral, J., Vidaurre, D., Marques, P., Magalhães, R., Moreira, P. S., Soares, J. M., ... Kringelbach, M. L. (2017). Cognitive performance in healthy older adults relates to spontaneous switching between states of functional connectivity during rest. *Scientific Reports*, *7*(1), 5135. <https://doi.org/10.1038/s41598-017-05425-7>
- Calhoun, V. D., Miller, R., Pearson, G., & Adahi, T. (2014). The chronnectome: Time-varying connectivity networks as the next frontier in fMRI data discovery. *Neuron*, *84*(2), 262–274. <https://doi.org/10.1016/j.neuron.2014.10.015>
- Chialvo, D. R. (2010). Emergent complex neural dynamics. *Nature Physics*, *6*(10), 744–750. <https://doi.org/10.1038/nphys1803>
- Chowdhury, F. A., Woldman, W., FitzGerald, T. H., Elwes, R. D., Nashef, L., Terry, J. R., & Richardson, M. P. (2014). Revealing a brain network endophenotype in families with idiopathic generalised epilepsy. *PLoS ONE*, *9*(10), e110136. <https://doi.org/10.1371/journal.pone.0110136>
- Cohen, J. R. (2018). The behavioral and cognitive relevance of time-varying, dynamic changes in functional connectivity. *NeuroImage*, *180*, 515–525. <https://doi.org/10.1016/j.neuroimage.2017.09.036>
- Colclough, G. L., Woolrich, M. W., Tewarie, P. K., Brookes, M. J., Quinn, A. J., & Smith, S. M. (2016). How reliable are MEG resting-state connectivity metrics? *NeuroImage*, *138*, 284–293. <https://doi.org/10.1016/j.neuroimage.2016.05.070>
- Da Silva, F. L., Blanes, W., Kalitzin, S. N., Parra, J., Suffczynski, P., & Velis, D. N. (2003). Epilepsies as dynamical diseases of brain systems: Basic models of the transition between normal and epileptic activity. *Epilepsia*, *44*, 72–83. <https://doi.org/10.1111/j.0013-9580.2003.12005.x>
- Dalkic, E. B. (2017). Neurostimulation devices used in treatment of epilepsy. *Current Treatment Options in Neurology*, *19*(2), 7. <https://doi.org/10.1007/s11940-017-0442-9>
- De Domenico, M., Solé-Ribalta, A., Cozzo, E., Kivela, M., Moreno, Y., Porter, M. A., ... Arenas, A. (2013). Mathematical formulation of multilayer networks. *Physical Review X*, *3*(4), 041022. <https://doi.org/10.1103/PhysRevX.3.041022>
- Duncan, J. S., Winston, G. P., Koeppe, M. J., & Ourselin, S. (2016). Brain imaging in the assessment for epilepsy surgery. *The Lancet Neurology*, *15*(4), 420–433. [https://doi.org/10.1016/S1474-4422\(15\)00383-X](https://doi.org/10.1016/S1474-4422(15)00383-X)
- Eavani, H., Satterthwaite, T. D., Gur, R. E., Gur, R. C., & Davatzikos, C. (2013). Unsupervised learning of functional network dynamics in resting state fMRI. In *International Conference on Information Processing in Medical Imaging* (pp. 426–437). Berlin: Springer. [https://doi.org/10.1007/978-3-642-38868-2\\_36](https://doi.org/10.1007/978-3-642-38868-2_36)
- Eckmann, J. P., Kamphorst, S. O., & Ruelle, D. (1987). Recurrence plots of dynamical systems. *Europhysics Letters (EPL)*, *5*, 973–977. <https://doi.org/10.1209/0295-5075/4/9/004>
- Eckmann, J. P., Kamphorst, S. O., & Ruelle, D. (1995). Recurrence plots of dynamical systems. *World Scientific Series on Nonlinear Science Series A Monographs Treatises*, *16*, 441–446.
- Engel, A. K., Gerloff, C., Hilgetag, C. C., & Nolte, G. (2013). Intrinsic coupling modes: Multiscale interactions in ongoing brain activity. *Neuron*, *80*(4), 867–886. <https://doi.org/10.1016/j.neuron.2013.09.038>
- Ezaki, T., Dos Reis, E. F., Watanabe, T., Sakaki, M., & Masuda, N. (2020). Closer to critical resting-state neural dynamics in individuals with higher fluid intelligence. *Communications Biology*, *3*(1), 1–9. <https://doi.org/10.1038/s42003-020-0774-y>
- Fornito, A., Zalesky, A., & Bullmore, E. (2016). *Fundamentals of brain network analysis*. London, UK: Academic Press. <https://doi.org/10.1016/C2012-0-06036-X>
- Fuertinger, S., Simonyan, K., Sperling, M. R., Sharan, A. D., & Hamzei-Sichani, F. (2016). High-frequency brain networks undergo modular breakdown during epileptic seizures. *Epilepsia*, *57*(7), 1097–1108. <https://doi.org/10.1111/epi.13413>
- Goodfellow, M., Rummel, C., Abela, E., Richardson, M. P., Schindler, K., & Terry, J. R. (2016). Estimation of brain network ictogenicity predicts outcome from epilepsy surgery. *Scientific Reports*, *6*, 29215. <https://doi.org/10.1038/srep29215>
- Guggisberg, A. G., Rizk, S., Ptak, R., Di Pietro, M., Saj, A., Lazeyras, F., ... Pignat, J. M. (2015). Two intrinsic coupling types for resting-state integration in the human brain. *Brain Topography*, *28*(2), 318–329. <https://doi.org/10.1007/s10548-014-0394-2>
- Hipp, J. F., Hawellek, D. J., Corbetta, M., Siegel, M., & Engel, A. K. (2012). Large-scale cortical correlation structure of spontaneous oscillatory activity. *Nature Neuroscience*, *15*(6), 884–890. <https://doi.org/10.1038/nn.3101>
- Holmes, G. L. (2015). Cognitive impairment in epilepsy: The role of network abnormalities. *Epileptic Disorders*, *17*(2), 101–116. <https://doi.org/10.1684/epd.2015.0739>
- Hutchison, R. M., Womelsdorf, T., Allen, E. A., Bandettini, P. A., Calhoun, V. D., Corbetta, M., ... Chang, C. (2013). Dynamic functional connectivity: Promise, issues, and interpretations. *NeuroImage*, *80*, 360–378. <https://doi.org/10.1016/j.neuroimage.2013.05.079>
- Jory, C., Shankar, R., Coker, D., McLean, B., Hanna, J., & Newman, C. (2016). Safe and sound? A systematic literature review of seizure detection methods for personal use. *Seizure*, *36*, 4–15. <https://doi.org/10.1016/j.seizure.2016.01.013>
- Khambhati, A. N., Davis, K. A., Oommen, B. S., Chen, S. H., Lucas, T. H., Litt, B., & Bassett, D. S. (2015). Dynamic network drivers of seizure generation, propagation and termination in human neocortical epilepsy. *PLoS Computational Biology*, *11*(12), e1004608. <https://doi.org/10.1371/journal.pcbi.1004608>
- Kini, L. G., Bernabei, J. M., Mikhail, F., Hadar, P., Shah, P., Khambhati, A. N., ... Litt, B. (2019). Virtual resection predicts surgical outcome for drug-resistant epilepsy. *Brain*, *142*(12), 3892–3905. <https://doi.org/10.1093/brain/awz303>
- Kitzbichler, M. G., Smith, M. L., Christensen, S. R., & Bullmore, E. (2009). Broadband criticality of human brain network synchronization. *PLoS Computational Biology*, *5*(3), e1000314. <https://doi.org/10.1371/journal.pcbi.1000314>
- Kivela, M., Arenas, A., Barthelemy, M., Gleeson, J. P., Moreno, Y., & Porter, M. A. (2014). Multilayer networks. *Journal of Complex Networks*, *2*(3), 203–271. <https://doi.org/10.1093/comnet/cnu016>
- Kramer, M. A., Eden, U. T., Kolaczyk, E. D., Zepeda, R., Eskandar, E. N., & Cash, S. S. (2010). Coalescence and fragmentation of cortical

- networks during focal seizures. *Journal of Neuroscience*, 30(30), 10076–10085. <https://doi.org/10.1523/JNEUROSCI.6309-09.2010>
- Krzemiński, D., Masuda, N., Hamandi, K., Singh, K. D., Routley, B., & Zhang, J. (2020). Energy landscape of resting magnetoencephalography reveals frontoparietal network impairments in epilepsy. *Network Neuroscience*, 4(2), 374–396. [https://doi.org/10.1162/netn\\_a\\_00125](https://doi.org/10.1162/netn_a_00125)
- Kurmukov, A., Dodonova, Y., & Zhukov, L. (2016). Classification of normal and pathological brain networks based on similarity in graph partitions. In *2016 IEEE 16th International Conference on Data Mining Workshops* (pp. 107–112). IEEE. <https://doi.org/10.1109/ICDMW.2016.0023>
- Lehnertz, K., Ansmann, G., Bialonski, S., Dickten, H., Geier, C., & Porz, S. (2014). Evolving networks in the human epileptic brain. *Physica D: Nonlinear Phenomena*, 267, 7–15. <https://doi.org/10.1016/j.physd.2013.06.009>
- Leijten, F. S., Dutch TeleEpilepsy Consortium, van Andel, J., Ungureanu, C., Arends, J., & Tan, F., ... de Weerd, A. (2018). Multimodal seizure detection: A review. *Epilepsia*, 59, 42–47. <https://doi.org/10.1111/epi.14047>
- Livi, L., & Rizzi, A. (2013). The graph matching problem. *Pattern Analysis and Applications*, 16(3), 253–283. <https://doi.org/10.1007/s10044-012-0284-8>
- Lopes, M. A., Richardson, M. P., Abela, E., Rummel, C., Schindler, K., Goodfellow, M., & Terry, J. R. (2017). An optimal strategy for epilepsy surgery: Disruption of the rich-club? *PLoS Computational Biology*, 13(8), e1005637. <https://doi.org/10.1371/journal.pcbi.1005637>
- Lopes, M. A., Richardson, M. P., Abela, E., Rummel, C., Schindler, K., Goodfellow, M., & Terry, J. R. (2018). Elevated ictal brain network ictogenicity enables prediction of optimal seizure control. *Frontiers in Neurology*, 9, 98. <https://doi.org/10.3389/fneur.2018.00098>
- Marwan, N., Donges, J. F., Zou, Y., Donner, R. V., & Kurths, J. (2009). Complex network approach for recurrence analysis of time series. *Physics Letters A*, 373(46), 4246–4254. <https://doi.org/10.1016/j.physleta.2009.09.042>
- Marwan, N., Romano, M. C., Thiel, M., & Kurths, J. (2007). Recurrence plots for the analysis of complex systems. *Physics Reports*, 438(5–6), 237–329. <https://doi.org/10.1016/j.physrep.2006.11.001>
- Miller, B. A., Stephens, L. H., & Bliss, N. T. (2012). Goodness-of-fit statistics for anomaly detection in Chung-Lu random graphs. In *2012 IEEE International Conference on Acoustics, Speech and Signal Processing* (pp. 3265–3268). IEEE. <https://doi.org/10.1109/ICASSP.2012.6288612>
- Morrell, M. (2006). Brain stimulation for epilepsy: Can scheduled or responsive neurostimulation stop seizures? *Current Opinion in Neurology*, 19(2), 164–168. <https://doi.org/10.1097/01.wco.0000218233.60217.84>
- Newman, M. E. J. (2006). Finding community structure in networks using the eigenvectors of matrices. *Physical Review E*, 74(3), 036104. <https://doi.org/10.1103/PhysRevE.74.036104>
- Ngamga, E. J., Bialonski, S., Marwan, N., Kurths, J., Geier, C., & Lehnertz, K. (2016). Evaluation of selected recurrence measures in discriminating pre-ictal and inter-ictal periods from epileptic EEG data. *Physics Letters A*, 380(16), 1419–1425. <https://doi.org/10.1016/j.physleta.2016.02.024>
- Nolte, G. (2003). The magnetic lead field theorem in the quasi-static approximation and its use for magnetoencephalography forward calculation in realistic volume conductors. *Physics in Medicine & Biology*, 48(22), 3637–3652. <https://doi.org/10.1088/0031-9155/48/22/002>
- Oostenveld, R., Fries, P., Maris, E., & Schoffelen, J. M. (2011). FieldTrip: Open source software for advanced analysis of MEG, EEG, and invasive electrophysiological data. *Computational Intelligence and Neuroscience*, 2011, 1. <https://doi.org/10.1155/2011/156869>
- Ouyang, G., Li, X., Dang, C., & Richards, D. A. (2008). Using recurrence plot for determinism analysis of EEG recordings in genetic absence epilepsy rats. *Clinical Neurophysiology*, 119(8), 1747–1755. <https://doi.org/10.1016/j.clinph.2008.04.005>
- Richardson, M. P. (2012). Large scale brain models of epilepsy: Dynamics meets connectomics. *Journal of Neurology, Neurosurgery and Psychiatry*, 83(12), 1238–1248. <https://doi.org/10.1136/jnnp-2011-301944>
- Rosch, R., Baldeweg, T., Moeller, F., & Baier, G. (2018). Network dynamics in the healthy and epileptic developing brain. *Network Neuroscience*, 2(1), 41–59. [https://doi.org/10.1162/NETN\\_a\\_00026](https://doi.org/10.1162/NETN_a_00026)
- Rummel, C., Abela, E., Andrzejak, R. G., Hauf, M., Pollo, C., Müller, M., ... Schindler, K. (2015). Resected brain tissue, seizure onset zone and quantitative EEG measures: Towards prediction of post-surgical seizure control. *PLoS ONE*, 10(10), e0141023. <https://doi.org/10.1371/journal.pone.0141023>
- Rummel, C., Müller, M., Baier, G., Amor, F., & Schindler, K. (2010). Analyzing spatio-temporal patterns of genuine cross-correlations. *Journal of Neuroscience Methods*, 191(1), 94–100. <https://doi.org/10.1016/j.jneumeth.2010.05.022>
- Schindler, K. A., Bialonski, S., Horstmann, M. T., Elger, C. E., & Lehnertz, K. (2008). Evolving functional network properties and synchronizability during human epileptic seizures. *Chaos*, 18(3), 033119. <https://doi.org/10.1063/1.2966112>
- Schmidt, H., Woldman, W., Goodfellow, M., Chowdhury, F. A., Koutroumanidis, M., Jewell, S., ... Terry, J. R. (2016). A computational biomarker of idiopathic generalized epilepsy from resting state EEG. *Epilepsia*, 57(10), e200–e204. <https://doi.org/10.1111/epi.13481>
- Shabani, H., Mikaili, M., & Noori, S. M. R. (2016). Assessment of recurrence quantification analysis (RQA) of EEG for development of a novel drowsiness detection system. *Biomedical Engineering Letters*, 6(3), 196–204. <https://doi.org/10.1007/s13534-016-0223-5>
- Sizemore, A. E., & Bassett, D. S. (2018). Dynamic graph metrics: Tutorial, toolbox, and tale. *NeuroImage*, 180, 417–427. <https://doi.org/10.1016/j.neuroimage.2017.06.081>
- Smith, S. J. M. (2005). EEG in the diagnosis, classification, and management of patients with epilepsy. *Journal of Neurology, Neurosurgery and Psychiatry*, 76(suppl 2), ii2–ii7. <https://doi.org/10.1136/jnnp.2005.069245>
- Sourty, M., Thoraval, L., Roquet, D., Armspach, J. P., Foucher, J., & Blanc, F. (2016). Identifying dynamic functional connectivity changes in dementia with lewy bodies based on product hidden markov models. *Frontiers in Computational Neuroscience*, 10, 60. <https://doi.org/10.3389/fncom.2016.00060>
- Sporns, O. (2013). Structure and function of complex brain networks. *Dialogues in Clinical Neuroscience*, 15(3), 247.
- Stahn, K., & Lehnertz, K. (2017). Surrogate-assisted identification of influences of network construction on evolving weighted functional networks. *Chaos*, 27(12), 123106. <https://doi.org/10.1063/1.4996980>
- Stam, C. J. (2014). Modern network science of neurological disorders. *Nature Reviews Neuroscience*, 15(10), 683–695. <https://doi.org/10.1038/nrn3801>
- Stam, C. J., Nolte, G., & Daffertshofer, A. (2007). Phase lag index: Assessment of functional connectivity from multi channel EEG and MEG with diminished bias from common sources. *Human Brain Mapping*, 28(11), 1178–1193. <https://doi.org/10.1002/hbm.20346>

- Tewarie, P., Hillebrand, A., van Dijk, B. W., Stam, C. J., O'Neill, G. C., Van Mieghem, P., ... Brookes, M. J. (2016). Integrating cross-frequency and within band functional networks in resting-state MEG: A multi-layer network approach. *NeuroImage*, *142*, 324–336. <https://doi.org/10.1016/j.neuroimage.2016.07.057>
- Vidaurre, D., Abeyesuriya, R., Becker, R., Quinn, A. J., Alfaro-Almagro, F., Smith, S. M., & Woolrich, M. W. (2018). Discovering dynamic brain networks from big data in rest and task. *NeuroImage*, *180*, 646–656. <https://doi.org/10.1016/j.neuroimage.2017.06.077>
- Webber Jr., C. L., & Marwan, N. (2015). *Recurrence quantification analysis. Theory and best practices*. Cham: Springer. <https://doi.org/10.1007/978-3-319-07155-8>
- Wilson, R. C., & Zhu, P. (2008). A study of graph spectra for comparing graphs and trees. *Pattern Recognition*, *41*(9), 2833–2841. <https://doi.org/10.1016/j.patcog.2008.03.011>
- Yan, X., Feng, S., Dai, J., & Wang, J. (2016). Detecting epileptic electroencephalogram by recurrence quantification analysis. In *2016 9th International Congress on Image and Signal Processing, BioMedical Engineering and Informatics* (pp. 1482–1486). IEEE. <https://doi.org/10.1109/CISP-BMEI.2016.7852951>
- Yang, C., Luan, G., Liu, Z., & Wang, Q. (2019). Dynamical analysis of epileptic characteristics based on recurrence quantification of SEEG recordings. *Physica A: Statistical Mechanics and its Applications*, *523*, 507–515. <https://doi.org/10.1016/j.physa.2019.02.017>

## SUPPORTING INFORMATION

Additional supporting information may be found online in the Supporting Information section.

**How to cite this article:** Lopes MA, Zhang J, Krzemiński D, et al. Recurrence quantification analysis of dynamic brain networks. *Eur J Neurosci*. 2020;00:1–20. <https://doi.org/10.1111/ejn.14960>